Influence of an urban canopy model and PBL schemes on vertical mixing for air quality modeling over Greater Paris

Youngseob Kim, Karine Sartelet, Jean-Christophe Raut, Patrick Chazette

Atmospheric Environment 107 (2015) 289–306

Contents lists available at ScienceDirect

Atmospheric Environment

journal homepage: www.elsevier.com/locate/atmosenv

Influence of an urban canopy model and PBL schemes on vertical mixing for air quality modeling over Greater Paris

Youngseob Kim [a, *], Karine Sartelet [a], Jean-Christophe Raut [b], Patrick Chazette [c]

[a] CEREA, Joint Research Laboratory, École des Ponts ParisTech/EDF R&D, Université Paris-Est, 6-8 Avenue Blaise Pascal, Cité Descartes, Champs-sur-Marne, 77455 Marne la Vallée Cedex 2, France
[b] Sorbonne Universités, UPMC Univ. Paris 06; Université Versailles St-Quentin; CNRS/INSU, LATMOS-IPSL, Paris, France
[c] Laboratoire des Sciences du Climat et de l'Environnement (LSCE), Laboratoire mixte CEA-CNRS-UVSQ, CEA Saclay, 91191 Gif-sur-Yvette, France

HIGHLIGHTS

- Improved PM_{10} vertical dispersion by urban canopy model (UCM) and Corine land-use.
- Higher influence of using UCM than different planetary boundary layer (PBL) schemes.
- Uncertainties of PM_{10} distribution related to the PBL height and PM_{10} emissions.
- Significant influences of vertical mixing on PM_{10} vertical dispersion.

ARTICLE INFO

Article history:
Received 25 September 2014
Received in revised form
12 December 2014
Accepted 4 February 2015
Available online 25 February 2015

Keywords:
Urban air quality modeling
PM_{10} vertical distribution
PBL parameterization
Urban canopy model
Eddy–diffusion coefficient
Polyphemus
Greater Paris

ABSTRACT

Impacts of meteorological modeling in the planetary boundary layer (PBL) and urban canopy model (UCM) on the vertical mixing of pollutants are studied. Concentrations of gaseous chemical species, including ozone (O_3) and nitrogen dioxide (NO_2), and particulate matter over Paris and the near suburbs are simulated using the 3-dimensional chemistry-transport model Polair3D of the Polyphemus platform. Simulated concentrations of O_3, NO_2 and PM_{10}/$PM_{2.5}$ (particulate matter of aerodynamic diameter lower than 10 μm/2.5 μm, respectively) are first evaluated using ground measurements. Higher surface concentrations are obtained for PM_{10}, $PM_{2.5}$ and NO_2 with the MYNN PBL scheme than the YSU PBL scheme because of lower PBL heights in the MYNN scheme. Differences between simulations using different PBL schemes are lower than differences between simulations with and without the UCM and the Corine land-use over urban areas. Regarding the root mean square error, the simulations using the UCM and the Corine land-use tend to perform better than the simulations without it. At urban stations, the PM_{10} and $PM_{2.5}$ concentrations are over-estimated and the over-estimation is reduced using the UCM and the Corine land-use. The ability of the model to reproduce vertical mixing is evaluated using NO_2 measurement data at the upper air observation station of the Eiffel Tower, and measurement data at a ground station near the Eiffel Tower. Although NO_2 is under-estimated in all simulations, vertical mixing is greatly improved when using the UCM and the Corine land-use. Comparisons of the modeled PM_{10} vertical distributions to distributions deduced from surface and mobile lidar measurements are performed. The use of the UCM and the Corine land-use is crucial to accurately model PM_{10} concentrations during nighttime in the center of Paris. In the nocturnal stable boundary layer, PM_{10} is relatively well modeled, although it is over-estimated on 24 May and under-estimated on 25 May. However, PM_{10} is under-estimated on both days in the residual layer, and over-estimated on both days over the residual layer. The under-estimations in the residual layer are partly due to difficulties to estimate the PBL height, to an over-estimation of vertical mixing during nighttime at high altitudes and to uncertainties in PM_{10} emissions. The PBL schemes and the UCM influence the PM vertical distributions not only because they influence vertical mixing (PBL height and eddy–diffusion coefficient), but also horizontal wind fields and

* Corresponding author.
E-mail addresses: kimy@cerea.enpc.fr (Y. Kim), sartelet@cerea.enpc.fr (K. Sartelet), jean-christophe.raut@latmos.ipsl.fr (J.-C. Raut), patrick.chazette@lsce.ipsl.fr (P. Chazette).

http://dx.doi.org/10.1016/j.atmosenv.2015.02.011

humidity. However, for the UCM, it is the influence on vertical mixing that impacts the most the PM_{10} vertical distribution below 1.5 km.

1. Introduction

Uncertainties of chemistry-transport models (CTM) have diverse origins: physico-chemical parameterizations (vertical dispersion, deposition velocities, chemical mechanism, etc.), input data (land-use data, emission inventories, meteorological fields, chemical kinetic constants, etc.) and numerical approximations (grid sizes, time steps, etc.). According to Mallet and Sportisse (2006), Roustan et al. (2010) and Tang et al. (2011), the largest uncertainties for ozone (O_3) and particulate matter (PM) concentrations are related to vertical dispersion and the number of vertical levels.

The vertical dispersion in CTM is mostly controlled by the planetary boundary layer (PBL) height and a turbulent flux modeled by an eddy–diffusion coefficient (K_z). The meteorological fields including the PBL height and K_z are not directly calculated in CTM but they are obtained from meteorological models.

The PBL height and K_z are determined by the heat and momentum exchanges between the PBL and the surface. In meteorological models, they are calculated by a PBL scheme (parameterization) and, therefore, the choice of the PBL scheme plays an important role (Borge et al., 2008; Kim et al., 2010, 2013). De Meij et al. (2009) and Appel et al. (2010) presented the influences of meteorological models on PM concentrations. They estimated that uncertainties of PBL heights from the different models are one of the major sources of the differences in the PM concentrations.

In strongly urbanized areas, the PBL height and K_z are significantly affected, particularly during nighttime, by anthropogenic heat release and geometric characteristics of urbanized areas, i.e., the existence of urban canopy, which lead to changes in vertical gradients of temperature and wind velocity (e.g., Dupont et al., 1999). To take into account the urban effects in meteorological models, urban canopy models have been developed (Kusaka et al., 2001; Martilli et al., 2002; Salamanca et al., 2010). Uno et al. (1989) and Dandou et al. (2005) showed that using urban canopy models leads to a significant increase of K_z during nighttime.

Various instrumented platforms have been used to investigate the vertical dispersion of pollutants in the PBL: fixed platforms (surface stations) and mobile platforms (automobile, aircraft, balloon, satellite, etc). Because of their capabilities of tracking the evolution of pollutants over time, lidars are widely employed on fixed platforms (Menut et al., 1999; Chen et al., 2001; Guibert et al., 2005; Chou et al., 2007), aircrafts (Flamant et al., 1997), satellites (Kaufman et al., 2003) or ground-based mobile platforms (Raut and Chazette, 2009; Royer et al., 2011). Some studies have included comparisons of measured and modeled vertical distribution of pollutants over Europe (Guibert et al., 2005) or Paris and its suburbs (Greater Paris) (Royer et al., 2011) during daytime. However, to our knowledge, there is no numerical study of the vertical distribution of pollutants in the nocturnal boundary layer and the residual layer over Greater Paris.

In our previous study (Kim et al., 2013), meteorological modeling in the PBL was performed over Greater Paris in May 2005 using the Weather Research and Forecast model (WRF) and the simulated meteorological fields were evaluated by comparison to observational data. The uncertainties linked to PBL schemes as well as to urban canopy modeling were investigated. It showed that urban canopy modeling is essential to reproduce the increase of the nocturnal PBL from the suburbs to the center of Paris. As the next step, the influence of urban canopy models on the vertical dispersion of pollutants is studied and compared to the influence of meteorological modeling in the PBL. To estimate the model performance, the modeled aerosol vertical distribution is compared to the distribution retrieved by a ground-based mobile lidar (GBML) system over Greater Paris during nighttime and early morning. First, a description of the model and the modeling setup is given. Then, simulations with different set-up (choice of PBL scheme and urban canopy model) are evaluated through comparisons of pollutant concentrations to observational data obtained by a surface measurement network, data at an upper air monitoring station, and lidar measurements. The comparisons to data are used to examine how concentrations are affected by the PBL scheme and the urban canopy model. The upper air observation station on the Eiffel Tower allows to gain more insights on the vertical structure of pollutants (nitrogen dioxide (NO_2) and O_3). The vertical distribution of PM_{10} (particles of aerodynamic diameter lower than 10 μm) concentrations are studied using data retrieved by the lidar. Finally, sensitivity studies are conducted to understand which meteorological fields mostly affect the PM_{10} vertical distribution when different PBL schemes and/or urban canopy modeling are used.

2. Model description and setup

2.1. Model description: Polyphemus

The chemistry-transport model Polair3D (Sartelet et al., 2007) of the air-quality platform Polyphemus version 1.6 (Mallet et al., 2007; http://cerea.enpc.fr/polyphemus) is used to model gaseous chemical species, including O_3, nitric oxide (NO) and NO_2, and PM. Within Polair3D/Polyphemus, the aerosol dynamics is modeled using SIREAM (Size REsolved Aerosol Model) (Debry et al., 2007) coupled to the Super-SORGAM secondary organic aerosol module (Kim et al., 2011) and the CB05 chemical kinetic mechanism (Yarwood et al., 2005). This modeling system has been successfully applied to Greater Paris to model PM_{10} vertical distribution during daytime (Royer et al., 2011).

2.2. Modeling domain and setup

Three modeling domains are used with one-way nesting (see Fig. 1). The largest domain covers western Europe and part of eastern Europe with a horizontal resolution of 0.5° × 0.5° (35.0° N – 70.0° N, 15.0° W – 35.0° E). The first nested domain covers France with a resolution of 0.125° × 0.125° (41.5° N – 51.1° N, 4.0° W – 10.1° E) and the smallest domain covers Greater Paris with a resolution of 0.02° × 0.02° (48.1° N – 49.2° N, 1.4° E – 3.5° E).

The vertical resolution of the three modeling domains consists of 21 levels defined at fixed altitudes above ground level (AGL), with a finer resolution near the surface. The altitudes of the vertical upper boundary of the grid cells are 40, 100, 200, 300, 400, 500, 600, 700, 800, 900, 1000, 1200, 1400, 1600, 1800, 2000, 2200, 2400, 3000, 4000, 6000 m AGL.

The simulation over Europe is carried out for one month from 1

May to 31 May 2005. The U.S. Geological Survey (USGS) land cover is used. Meteorological inputs are obtained from a reanalysis provided by the European Centre for Medium-Range Weather Forecasts (ECMWF). Anthropogenic emissions of gases and PM are generated with the European Monitoring and Evaluation Programme (EMEP) inventory for 2005. Biogenic emissions are computed as in Simpson et al. (1999) and sea-salt emissions as in Monahan et al. (1986). For initial conditions, lateral and top boundary conditions, daily means are extracted from the outputs of the global chemistry and aerosol model, Interaction Chimie-Aérosols (INCA) coupled to the Laboratoire de Météorologie Dynamique general circulation model (LMDz) for this study (http://www-lsceinca.cea.fr/).

The nested simulation over France is performed from 7 May to 31 May 2005. Meteorological inputs are obtained from the Fifth-Generation NCAR/Penn State Mesoscale Model (MM5) (Dudhia, 1993), with a horizontal resolution of 12 km and a vertical resolution of 29 levels between 0 m and 13,700 m. The cylindrical projection is used in the Polair3D simulation whereas the Lambert conformal conic (LCC) projection is used in the MM5 simulation. The meteorological data were converted from the LCC projection to the cylindrical projection. Initial and boundary conditions are extracted from outputs of the simulation over Europe.

The domain for the nested simulation over Greater Paris is presented in Fig. 2. Initial and boundary conditions are extracted from outputs of the simulation over France. Meteorological inputs are obtained from the WRF model version 3.3 with a horizontal resolution of 0.03125° and 24 vertical sigma levels between 18 m and 16,100 m AGL refined near the surface. There are five to six levels below 400 m (depending on topography), which represent the nocturnal boundary layer in this study. The WRF simulation over Greater Paris is detailed in the companion paper (Kim et al., 2013). Four WRF simulations are performed, changing the PBL scheme and with/without the urban canopy model (UCM, Kusaka et al., 2001). The two PBL schemes, which performed best in Kim et al. (2013) for meteorological modeling, are used: the Yonsei University (YSU) scheme (Hong et al., 2006), a nonlocal closure scheme, and the Mellor-Yamada-Nakanishi and Niino (MYNN) scheme (Nakanishi and Niino, 2004), a local closure scheme. Using the UCM in the WRF model leads to changes in the modeling of the meteorological fields, e.g., wind speed, temperature, humidity and PBL height. It affects the vertical distribution of atmospheric pollutants by modifying PBL height and mixing strength. Geometric (building height/width, road width, urban area ratio) and thermal parameters (anthropogenic heat, thermal conductivities, heat capacity) have a significant effect on UCM modeling. However, these parameters are attached to high uncertainties, and it is difficult to choose representative values, especially with a limited number of urban land-use types. The UCM parameters used here are the same as in Kim et al. (2013). Most of them are based on Kusaka et al. (2001). The annual anthropogenic heat release is 70 W m^{-2}, based on the work of Allen et al. (2011). Kusaka et al. (2001) showed that the diurnal variations of surface temperature from the UCM, which is a single-layer model, are close to those from multi-layer models. In addition, the UCM includes the anthropogenic heat release in the total sensible heat flux, which is not explicitly represented in the multi-layer models.

In Polair3D/Polyphemus, K_z is parameterized following Troen and Mahrt (1986) and Louis (1979). The parameterization of Louis (1979) is used to calculate the coefficients, except in the unstable convective boundary layer. The parameterization of Louis (1979) depends on the vertical gradient of the wind speed v as follows

$$K_z = l^2 F \left| \frac{\Delta v}{\Delta z} \right| \tag{1}$$

where l is the mixing length and F is the stability function. In the unstable convective boundary layer, the coefficients are calculated using the parameterization of Troen and Mahrt (1986), as it tends to be more robust for a fine discretization of vertical levels near the surface.

$$K_z = u_* \kappa z \Phi^{-1} \left(1 - \frac{z}{h}\right)^p \tag{2}$$

where u_* is the surface friction velocity, κ is the Von Kàrmàn

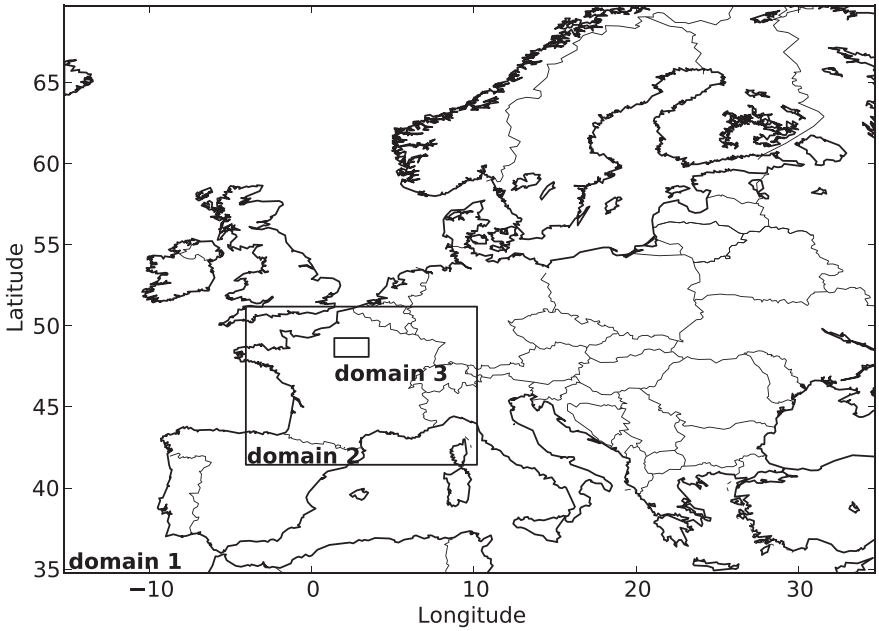

Fig. 1. Three modeling domains for Polair3D/Polyphemus simulations. The domain over Europe corresponds to domain 1 and the nested domains over France and Greater Paris correspond to domain 2 and 3, respectively.

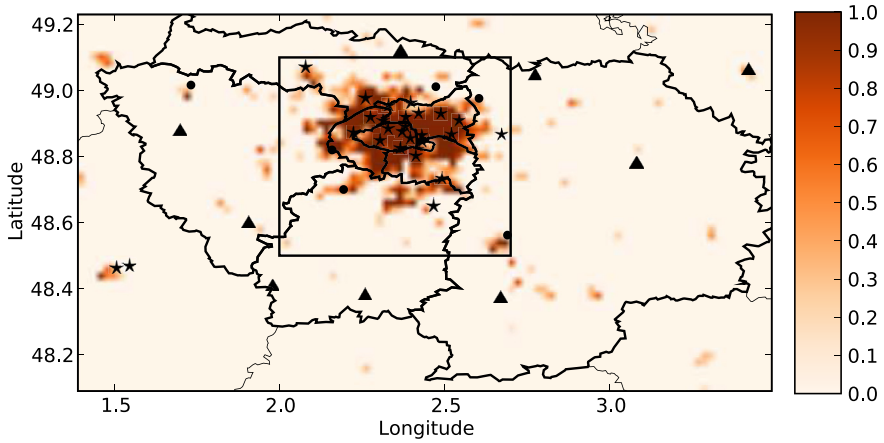

Fig. 2. Modeling domain over Greater Paris. The black lines show the geographical boundary of the administrative department and the thick lines correspond to the boundary of the departments in the Île-de-France region. Locations of the BDQA stations over Greater Paris are also presented: stars, circles and triangles show the urban, suburban and rural stations, respectively. The yellow gradation shows the urban fraction of the land-use data. The black box presents Paris and its near suburbs strongly urbanized. (For interpretation of the references to colour in this figure legend, the reader is referred to the web version of this article.)

constant set to 0.4, Φ is the non-dimensional shear, h is the PBL height and the exponent p is set to 2 for this study.

A preprocessing tool calculates K_z from modeled meteorological variables, such as wind velocity and PBL height, which are obtained from the WRF simulation. To estimate the influence of the K_z parameterization on the PM_{10} vertical distribution, the K_z extracted from outputs of the WRF simulations with the YSU and the MYNN schemes (K_z for heat) are compared to the K_z obtained from the Polyphemus preprocessing tool. A minimum value of K_z is set. This minimum K_z corresponds to a background diffusion, which is often used in PBL schemes to prevent numerical problems. It is also called numerical diffusion (Hong and Pan, 1996; Shin and Hong, 2011). When the Polyphemus preprocessing tool computes K_z, a minimum K_z is set as in the WRF PBL schemes for the sake of consistency. The minimum value of the coefficient is set to 10^{-6} m^2 s^{-1} except in the lowest layers (Pleim, 2011) where it is set to 0.2 m^2 s^{-1}.

2.3. Episode of the simulation over Greater Paris

The nested simulation over Greater Paris is carried out from 9 to 27 May. This simulation period was chosen because of the availability of measurements between 24 and 27 May 2005. The measurement campaign is introduced below in details.

The weather conditions (clear sky and weak winds) during this period were favorable to local-scale air quality study. Local-scale flow dominated the dispersion of pollutants because of weak synoptic flow. Strongly developed anticyclones prevented dispersion, led to low precipitation, resulting in high pollution levels.

2.4. AIRPARIF emission inventory

For the nested simulation over Greater Paris, anthropogenic emissions are generated with the AIRPARIF (air quality agency of the Paris region) inventory (http://www.airparif.asso.fr/) for 2005 over the Île-de-France region and with the EMEP inventory outside (see Fig. 3).

The AIRPARIF inventory includes emissions of nitrogen oxides (NO_x: NO and NO_2), sulfur dioxide (SO_2), carbon monoxide (CO), non-methane volatile organic compounds (NMVOC), PM_{10}, $PM_{2.5}$ (particulate matter of aerodynamic diameter lower than 2.5 μm), methane (CH_4) and ammonia (NH_3) from various sources: point sources, mobile sources (traffic, railroad and aircrafts) and fixed surface sources. Annual emissions are provided for different SNAP (Selected Nomenclature for sources of Air Pollution) categories. The annual emissions by SNAP categories are given in Table 1 (AIRPARIF, 2004). Road transport is the dominant category for NO_x (52%), CO (77%) and PM_{10} (36%) followed by non-industrial combustion plants. For NO_x, agricultural activities contribute about 10% of total emissions (including 3% for agricultural equipments in the category 'other mobile sources and machinery'). The AIRPARIF emission inventory covers Paris, its suburbs and outer rural regions (see Figs. 2 and 3). The significant contribution of agricultural activities on NO_x is due to this large coverage of the inventory. Major sources for emissions of NMVOC are solvent use (41%) and road transport (29%). SO_2 is emitted mostly by combustion in plants (energy: 41%, non-industrial: 42% and manufacturing: 10%).

Emissions are distributed over grid cells and diluted in the whole volume of the grid cells. The number of grid cells in the AIRPARIF inventory is 12,040 with a horizontal resolution of $0.0136° \times 0.009°$. For point sources and aircraft sources, the heights of the emissions are given in the inventory. However, for point sources, the effective height of emissions is computed taking into account plume rise following the parameterization of Briggs modified by Hanna and Paine (1989).

The temporal variations of emissions are obtained by applying temporal factors (monthly, daily and hourly) available from AIRPARIF to the annual emission data. These factors are available by SNAP categories. The temporal fractions of the annual emissions for May are presented in Table 1. A low fraction (4.6%) is used for the category 'Non-industrial combustion plants', which includes domestic heating, because of seasonally warm meteorological conditions.

The chemical speciation of VOC is given by the Institut für Energiewirtschaft und Rationelle Energieanwendung (IER, http://www.ier.uni-stuttgart.de/index.en.html) for simulations over Greater Paris and CORINAIR (CO-oRdinated INformation on the Environment in the European Community – AIR)'s speciation for simulations over Europe and France (EEA, 2006). The size distribution of primary PM are evaluated following EMEP guidelines (Simpson et al., 2003) and the chemical speciation of CityDelta for Milan is used (http://aqm.jrc.ec.europa.eu/citydelta/).

The limitations of this inventory are well described in AIRPARIF (2011). The PM chemical speciations are not provided and the volatility of primary organic aerosol is not taken into account (Couvidat et al., 2012). The inventory does not include dust resuspension which varies with meteorological conditions and biogenic

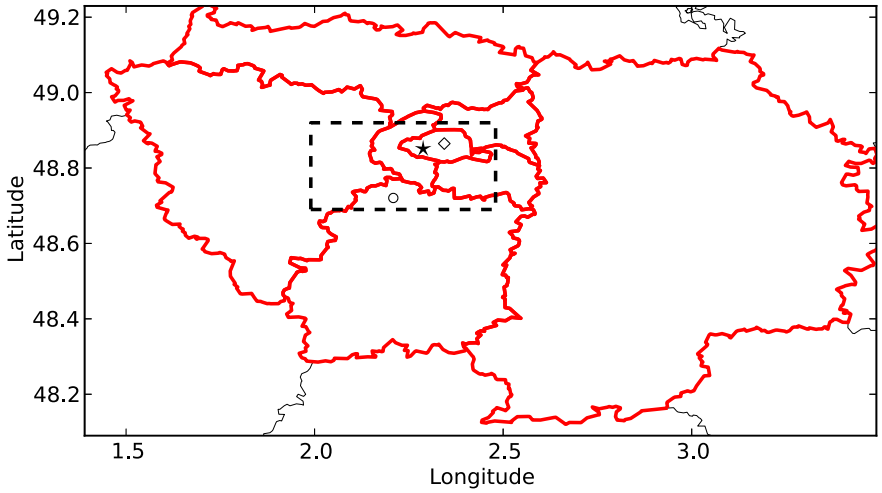

Fig. 3. Area covered by the AIRPARIF emission inventory in the modeling domain over Greater Paris (red lines). Measurement locations over Greater Paris are also presented: star (Paris-7 and Eiffel Tower), circle (Palaiseau) and diamond (Les Halles). Dashed rectangle corresponds to the limits of the area shown in Fig. 5. (For interpretation of the references to colour in this figure legend, the reader is referred to the web version of this article.)

Table 1
Annual emissions by SNAP categories using the AIRPARIF inventory in the year 2000 (ton yr^{-1}).

Category	NO_x	CO	SO_2	NMVOC	PM_{10}	Fraction for May (%)
Combustion in energy and transformation industries	15,641	4682	27,500	704	2025	5.2
Non-industrial combustion plants	19,345	69,010	28,473	13,434	6266	4.6
Combustion in manufacturing industry	7368	1000	6660	463	488	7.4
Production processes	299	3	354	1837	4009	8.3
Extraction & distribution of fossil fuels and geothermal energy	0	0	0	6569	0	0
Solvent and other product use	3	0	0	73,276	0	0
Road transport	84,178	306,341	2324	52,472	7998	8.4
Other mobile sources and machinery	14,656	15,086	553	3973	708	8.1
Waste treatment and disposal	7450	2297	1736	1742	546	8.3
Agriculture	12,441	0	0	0	71	9.4
Other sources and sinks	0	0	0	24,025	0	0

emissions.

2.5. Sensitivity runs

The Polair3D/Polyphemus simulations are labelled Reference-YSU and Reference-MYNN when meteorological fields are simulated without the UCM in the WRF simulation, but with the YSU and the MYNN schemes, respectively. When the UCM is used to compute meteorological fields in the WRF simulation, the recent Corine (Coordination of Information on the Environment) land-use data (http://www.eea.europa.eu/data-and-maps/data/corine-land-cover-2006-raster) is also used to take into account recent land-use changes over Greater Paris.

The Polyphemus simulations using outputs of the WRF simulation with the UCM and the Corine land-use are labelled UCM-Corine-YSU and UCM-Corine-MYNN. To test the sensitivity to the modeling of the K_z in the Polair3D/Polyphemus simulations using the K_z computed in the WRF simulations are also performed. They are labelled UCM-Corine-YSU-Kz and UCM-Corine-MYNN-Kz. The list of the conducted simulations with their characteristics is presented in Table 2.

3. Comparisons to observational data

3.1. Surface observations

We compare pollutant concentrations obtained from the simulations over Greater Paris (9–27 May) to a French surface observation database for air quality, Base de Données de la Qualité de l'Air (BDQA). There are five types of stations in the BDQA database: rural, suburban, urban, traffic and industrial stations (ADEME, 2002). Considering the representativeness of the types and the grid size of the simulations, only the rural, suburban and urban stations are taken into account in the comparisons. Hourly observations of PM_{10}, $PM_{2.5}$, O_3 and NO_2 are available for 2005. Details on the measurements are presented at http://www.atmonet.org/and the locations of the BDQA observation stations are displayed in Fig. 2. The statistical indicators used in this study are the root mean square error (RMSE), the mean fractional bias and error (MFB and MFE), and the mean normalized bias and gross error (MNB and MNGE). They are defined in Table 3. A cut-off value is typically applied to evaluate O_3 modeling performance for regulatory purposes (high O_3 concentrations). Because this study focuses on nighttime modeling (low O_3 concentrations), this cut-off value is not applied in this study except in Section 3.1.1. Modeled

Table 2
Characteristics of the simulations.

Name	PBL scheme	Using UCM	Land-use data	K_z computation
Reference-YSU	YSU	No	USGS	Polyphemus
Reference-MYNN	MYNN	No	USGS	Polyphemus
UCM-Corine-YSU	YSU	Yes	Corine	Polyphemus
UCM-Corine-MYNN	MYNN	Yes	Corine	Polyphemus
UCM-Corine-YSU-Kz	YSU	Yes	Corine	WRF
UCM-Corine-MYNN-Kz	MYNN	Yes	Corine	WRF

concentrations are compared to observations from the BDQA database in Tables 4a–4d.

3.1.1. Statistics averaged over all stations

For O_3, the MNGE of the four Polair3D/Polyphemus simulations varies between 0.14 and 0.17 using a 60 μg m^{-3} threshold, while the MNB varies between −0.07 and 0.02. These results meet performance standards, typically MNGE ≤ 0.3 and |MNB| ≤ 0.15 (Russell and Dennis, 2000). For PM_{10}, following Boylan and Russell (2006), the model performance goals (|MFB| ≤ 0.30 and MFE ≤ 0.50) and criteria (|MFB| ≤ 0.60 and MFE ≤ 0.75) are met for all four Polair3D/Polyphemus simulations. For $PM_{2.5}$, the model performance criteria are met for all 4 simulations, but the model performance goals are met for 3 simulations (Reference-YSU, UCM-Corine-YSU and UCM-Corine-MYNN). The MFB varies between 0.09 and 0.26 and the MFE between 0.43 and 0.46 for the 3 simulations. For the Reference-MYNN simulation, although the model performance goal is met for the MFE (0.48), it is not met for the MFB (0.32).

3.1.2. Variations of statistics with station types

The modeled concentrations in the Reference-YSU and UCM-Corine-YSU simulations are compared to the BDQA database at different types of stations (see Tables 4a–4d).

At urban stations, the modeled concentrations of PM_{10} and $PM_{2.5}$ in the Reference-YSU simulation are over-estimated. The over-estimation at urban stations is due to an under-estimated vertical mixing. The over-estimation is reduced with higher vertical mixing in the UCM-Corine-YSU simulation. At a suburban station (only one station is available for $PM_{2.5}$ measurements), the modeled concentration of $PM_{2.5}$ in the Reference-YSU simulation is over-estimated. However the PM_{10} concentration is under-estimated, partly because the $PM_{2.5}$ fraction of total PM_{10} is over-estimated in the modeling compared to observations. At rural stations, PM_{10} is under-estimated for both the Reference-YSU and UCM-Corine-YSU simulations. Slightly better statistics are obtained compared to suburban stations.

3.1.3. Variations of statistics with the PBL schemes

Statistics obtained with the Reference-YSU and Reference-MYNN simulations are compared. Using the MYNN scheme rather than the YSU scheme leads to higher surface concentrations for PM_{10}, $PM_{2.5}$ and NO_2, suggesting weaker vertical mixing near the surface. For PM_{10}, the statistics are better with the YSU scheme except for the MFB which is slightly better with the MYNN scheme. For $PM_{2.5}$, the statistics are better when the YSU scheme is used rather than the MYNN scheme because the over-estimation of $PM_{2.5}$ is lower with the YSU scheme. The YSU scheme better estimates O_3 and NO_2 concentrations. The differences in O_3 and NO_2 concentrations between the YSU and MYNN schemes are lower than those in PM_{10} and $PM_{2.5}$ concentrations.

Table 3
Definitions of the statistical indicators.

Indicators	Definitions
Root mean square error (RMSE)	$\sqrt{\frac{1}{n}\sum_{i=1}^{n}(c_i - o_i)^2}$
Mean fractional bias (MFB) and mean fractional error (MFE)	$\frac{1}{n}\sum_{i=1}^{n}\frac{c_i-o_i}{(c_i+o_i)/2}$ and $\frac{1}{n}\sum_{i=1}^{n}\frac{\lvert c_i-o_i\rvert}{(c_i+o_i)/2}$
Mean normalized bias (MNB) and mean normalized gross error (MNGE)	$\frac{1}{n}\sum_{i=1}^{n}\frac{c_i-o_i}{o_i}$ and $\frac{1}{n}\sum_{i=1}^{n}\frac{\lvert c_i-o_i\rvert}{o_i}$

c_i: modeled values, o_i: observed values, n: number of data.

3.1.4. Variations of statistics with the UCM and the Corine land-use

The impacts of the UCM and the Corine land-use on the mean concentrations of pollutants show a similar tendency at all types of stations (rural, suburban and urban) with lower surface concentrations for PM_{10}, $PM_{2.5}$ and NO_2 because of greater vertical mixing. Using the UCM and the Corine land-use, the PBL heights increase by as much as 75% for the YSU scheme and by more than a factor 3 for the MYNN scheme. The variations of O_3 evolve in opposite to the variations of NO_2. The amplitudes of the impacts are lower at rural stations (from 3% for PM_{10} to 12% for NO_2) than at urban stations (from 17% for PM_{10} to 28% for NO_2).

Differences between simulations using different PBL schemes (6% for PM_{10} and $PM_{2.5}$, 2% for O_3 and 4% for NO_2) are lower than differences between simulations with and without the UCM and the Corine land-use (using the YSU scheme, 14% for PM_{10}, 20% for $PM_{2.5}$, 12% for O_3 and 28% for NO_2 and using the MYNN scheme, 12% for PM_{10}, 17% for $PM_{2.5}$, 10% for O_3 and 22% for NO_2). Lower concentrations are obtained for PM_{10}, $PM_{2.5}$ and NO_2 in the UCM-Corine simulations and the statistics are globally improved. The lower concentrations at the surface stations in the UCM-Corine simulations are due to stronger vertical mixing. For $PM_{2.5}$, the UCM-Corine simulations perform better than the Reference simulations because the over-estimation of $PM_{2.5}$ is reduced. For PM_{10}, the UCM-Corine simulations give better statistics, except for the MFB. The modeled means are under-estimated in the UCM-Corine simulations, whereas they are well estimated in the Reference simulations. In opposite to PM_{10}, $PM_{2.5}$ and NO_2, for O_3 the UCM-Corine simulations lead to higher mean concentrations. This increase in O_3 concentration is due to the decrease in NO_2 concentration in the UCM-Corine simulations. The NO_2 concentrations at the urban station in Paris, Les Halles (Fig. 4) are significantly different during the morning rush hour between the Reference-YSU and UCM-Corine-YSU simulations. The peaks in the figure correspond to the increase of NO_2 during the rush hour according to the temporal variations of the NO_2 emissions. For the formation of O_3, as Paris is in a VOC-limited regime (Kim et al., 2009), an increase of NO_2 leads to a decrease of O_3 according to the O_3 isopleth of Seinfeld and Pandis (1998). As NO_2 is lower in the UCM-Corine-YSU simulation, O_3 is higher especially at night.

3.1.5. Impact of the eddy–diffusion coefficient

As shown Tables 4a–4d, the concentrations of PM_{10}, $PM_{2.5}$ and NO_2 in the UCM-Corine-YSU-Kz and UCM-Corine-MYNN-Kz simulations are systematically lower than those in the UCM-Corine-YSU and UCM-Corine-MYNN simulations, respectively because K_z are higher (see Fig. 6b, d, f, h). The concentrations of O_3 in the UCM-Corine-YSU-Kz and UCM-Corine-MYNN-Kz simulations tend to be higher than the UCM-Corine-YSU and UCM-Corine-MYNN simulations.

Comparisons of surface PM_{10} concentrations to measurements at the BDQA stations show that the UCM-Corine-MYNN-Kz and UCM-Corine-YSU-Kz simulations do not systematically perform better than the UCM-Corine-MYNN and UCM-Corine-YSU simulations. Although the UCM-Corine-MYNN-Kz and UCM-Corine-YSU-Kz simulations have slightly lower RMSE than the UCM-Corine-MYNN and UCM-Corine-YSU simulations, they also have higher bias as the mean PM_{10} concentrations are lower. However, for $PM_{2.5}$, the UCM-Corine-MYNN-Kz and UCM-Corine-YSU-Kz simulations perform better than the UCM-Corine-MYNN and UCM-Corine-YSU simulations, as modeled concentrations are lower. The opposite is observed for O_3 and NO_2 with better performance of the UCM-Corine-MYNN and UCM-Corine-YSU simulations.

3.1.6. Variations of statistics between daytime and nighttime

In Table 5, we present PM_{10} concentrations averaged over 11

Table 4a
Comparison of modeled concentrations to observations from the BDQA database: (a) PM_{10}, (b) $PM_{2.5}$, (c) O_3 and (d) NO_2. Mean statistical scores at all stations and scores at different station types (urban, suburban and rural) are presented.

Station type	Station number	Observed mean[a,b] ($\mu g\ m^{-3}$)	Model[c]	Modeled mean[a,b] ($\mu g\ m^{-3}$)	RMSE[a] ($\mu g\ m^{-3}$)	MFB[a]	MFE[a]	MNB[a]	MNGE[a]
Total	17	17.0	R-YSU	17.0	9.5	−0.06	0.41	0.08	0.44
			R-MYNN	18.0	10.1	0.00	0.41	0.16	0.47
			UC-YSU	14.6	8.4	−0.17	0.41	−0.05	0.39
			UC-MYNN	15.9	8.6	−0.09	0.40	0.03	0.41
			UC-YSU-Kz	14.1	8.3	−0.19	0.41	−0.08	0.39
			UC-MYNN-Kz	13.9	8.5	−0.20	0.42	−0.08	0.39
Urban	11	17.8	R-YSU	19.2	10.4	0.02	0.39	0.17	0.45
			R-MYNN	20.3	11.3	0.08	0.41	0.25	0.51
			UC-YSU	15.9	8.6	−0.13	0.39	−0.01	0.39
			UC-MYNN	17.5	9.0	−0.04	0.39	0.09	0.42
			UC-YSU-Kz	15.4	8.5	−0.15	0.39	−0.04	0.38
			UC-MYNN-Kz	15.0	8.9	−0.17	0.41	−0.05	0.39
Suburban	3	17.0	R-YSU	14.1	9.0	−0.21	0.45	−0.08	0.41
			R-MYNN	15.1	8.8	−0.14	0.41	−0.01	0.40
			UC-YSU	12.8	9.0	−0.29	0.46	−0.16	0.39
			UC-MYNN	13.8	8.7	−0.22	0.43	−0.10	0.38
			UC-YSU-Kz	12.3	9.0	−0.32	0.47	−0.19	0.39
			UC-MYNN-Kz	12.5	9.0	−0.31	0.46	−0.18	0.39
Rural	3	13.7	R-YSU	11.7	7.0	−0.20	0.43	−0.08	0.39
			R-MYNN	12.4	7.0	−0.13	0.41	0.0	0.40
			UC-YSU	11.3	6.9	−0.22	0.43	−0.10	0.39
			UC-MYNN	12.1	6.7	−0.14	0.40	−0.03	0.38
			UC-YSU-Kz	11.2	6.8	−0.22	0.43	−0.10	0.38
			UC-MYNN-Kz	11.4	6.7	−0.20	0.41	−0.09	0.37

[a] Mean values over all stations. The statistical indicators are calculated for each station and then they are arithmetically averaged.
[b] Mean concentrations from 9 to 27 May.
[c] R-YSU: Reference-YSU, R-MYNN: Reference-MYNN, UC-YSU: UCM-Corine-YSU, UC-MYNN: UCM-Corine-MYNN, UC-YSU-Kz: UCM-Corine-Kz and UC-MYNN-Kz: UCM-Corine-MYNN-Kz.

urban stations. The daily mean concentrations are compared to those calculated during daytime (0800 UTC to 2000 UTC) and nighttime (2100 UTC to 0700 UTC of next day). The PM_{10} concentrations with the Reference-YSU and Reference-MYNN simulations are over-estimated during nighttime. The over-estimation during nighttime are significantly reduced using the UCM and the Corine land-use. However the concentrations during daytime are also influenced by using the UCM and the Corine land-use and under-estimated. The under-estimation of PM_{10} during daytime implies that the emission inventory may need improvements as discussed in Section 3.3.2.

3.2. Upper air observations: the Eiffel Tower

Although the stations included in the BDQA database are surface stations, AIRPARIF (http://www.airparif.asso.fr/) monitors the upper air quality with a station located at the fourth floor (319 m AGL) of the Eiffel Tower. It is useful to compare the concentration at the Eiffel Tower (hereafter Eiffel) to a nearby surface station (Paris-7) to diagnose the vertical distribution of pollutants, although only NO_2 is monitored at Paris-7. The station Paris-7 is an urban background station which is situated in urban center and sufficiently distant from road traffic. The locations of the monitoring stations are presented in Fig. 5. Modeled concentrations are compared to observations at Eiffel and Paris-7 in Table 6.

The Reference-YSU and Reference-MYNN simulations lead to

Table 4b
Comparison of modeled concentrations to observations from the BDQA database: (a) PM_{10}, (b) $PM_{2.5}$, (c) O_3 and (d) NO_2. Mean statistical scores at all stations and scores at different station types (urban, suburban and rural) are presented.

Station type	Station number	Observed mean[a,b] ($\mu g\ m^{-3}$)	Model	Modeled mean[a,b] ($\mu g\ m^{-3}$)	RMSE[a] ($\mu g\ m^{-3}$)	MFB[a]	MFE[a]	MNB[a]	MNGE[a]
Total	5	11.1	R-YSU	15.5	9.7	0.26	0.46	0.53	0.70
			R-MYNN	16.5	10.7	0.32	0.48	0.64	0.78
			UC-YSU	12.4	6.9	0.09	0.43	0.27	0.53
			UC-MYNN	13.7	7.8	0.17	0.45	0.40	0.62
			UC-YSU-Kz	11.7	6.3	0.04	0.41	0.20	0.48
			UC-MYNN-Kz	11.1	6.1	−0.01	0.41	0.14	0.47
Urban	4	11.5	R-YSU	16.4	10.4	0.28	0.47	0.57	0.72
			R-MYNN	17.5	11.6	0.34	0.49	0.69	0.81
			UC-YSU	12.9	7.1	0.10	0.43	0.28	0.54
			UC-MYNN	14.4	8.2	0.19	0.46	0.42	0.63
			UC-YSU-Kz	12.2	6.5	0.05	0.40	0.21	0.49
			UC-MYNN-Kz	11.5	6.2	0.00	0.41	0.16	0.47
Suburban	1	9.8	R-YSU	12.0	7.3	0.15	0.45	0.40	0.62
			R-MYNN	12.7	7.3	0.22	0.45	0.46	0.64
			UC-YSU	10.5	6.0	0.05	0.43	0.22	0.52
			UC-MYNN	11.1	6.3	0.10	0.44	0.30	0.56
			UC-YSU-Kz	9.8	5.6	−0.01	0.41	0.14	0.46
			UC-MYNN-Kz	9.4	5.4	−0.05	0.42	0.10	0.46

[a], [b], [c]: for the detailed caption of the table, see Table 4a.

Table 4c
Comparison of modeled concentrations to observations from the BDQA database: (a) PM_{10}, (b) $PM_{2.5}$, (c) O_3 and (d) NO_2. Mean statistical scores at all stations and scores at different station types (urban, suburban and rural) are presented.

Station type	Station number	Observed mean[a,b] (μg m^{-3})	Model	Modeled mean[a,b] (μg m^{-3})	RMSE[a] (μg m^{-3})	MFB[a]	MFE[a]	MNB[a]	MNGE[a]
Total	30	56.4	R-YSU	61.9	22.6	0.11	0.38	0.46	0.66
			R-MYNN	60.9	23.3	0.09	0.39	0.46	0.67
			UC-YSU	69.5	25.7	0.28	0.39	0.83	0.92
			UC-MYNN	66.7	24.7	0.23	0.38	0.71	0.83
			UC-YSU-Kz	71.0	26.5	0.31	0.40	0.88	0.95
			UC-MYNN-Kz	70.0	25.5	0.30	0.39	0.89	0.96
Urban	16	53.6	R-YSU	57.5	22.4	0.06	0.42	0.43	0.68
			R-MYNN	55.7	23.1	0.02	0.43	0.40	0.68
			UC-YSU	67.7	26.4	0.30	0.43	0.97	1.06
			UC-MYNN	63.9	25.4	0.23	0.41	0.80	0.93
			UC-YSU-Kz	68.7	26.7	0.32	0.43	1.00	1.08
			UC-MYNN-Kz	70.0	27.5	0.36	0.44	1.14	1.20
Suburban	5	58.3	R-YSU	64.1	22.5	0.15	0.36	0.48	0.64
			R-MYNN	63.6	23.0	0.14	0.36	0.50	0.67
			UC-YSU	72.2	26.0	0.30	0.38	0.85	0.91
			UC-MYNN	68.6	23.8	0.24	0.35	0.68	0.78
			UC-YSU-Kz	73.2	26.6	0.31	0.39	0.86	0.93
			UC-MYNN-Kz	71.7	24.9	0.29	0.37	0.80	0.86
Rural	9	60.2	R-YSU	68.6	23.1	0.19	0.33	0.51	0.63
			R-MYNN	68.7	24.0	0.19	0.35	0.53	0.66
			UC-YSU	71.4	24.2	0.24	0.34	0.59	0.67
			UC-MYNN	70.6	24.2	0.23	0.34	0.57	0.67
			UC-YSU-Kz	74.0	26.1	0.28	0.36	0.67	0.74
			UC-MYNN-Kz	68.9	22.1	0.20	0.32	0.49	0.59

[a], [b], [c]: for the detailed caption of the table, see Table 4a.

Table 4d
Comparison of modeled concentrations to observations from the BDQA database: (a) PM_{10}, (b) $PM_{2.5}$, (c) O_3 and (d) NO_2. Mean statistical scores at all stations and scores at different station types (urban, suburban and rural) are presented.

Station type	Station number	Observed mean[a,b] (μg m^{-3})	Model	Modeled mean[a,b] (μg m^{-3})	RMSE[a] (μg m^{-3})	MFB[a]	MFE[a]	MNB[a]	MNGE[a]
Total	32	28.2	R-YSU	27.7	18.9	−0.15	0.54	0.14	0.64
			R-MYNN	28.8	19.0	−0.11	0.53	0.18	0.64
			UC-YSU	19.9	18.0	−0.42	0.64	−0.15	0.57
			UC-MYNN	22.5	17.8	−0.31	0.59	−0.05	0.57
			UC-YSU-Kz	18.9	18.2	−0.47	0.66	−0.19	0.57
			UC-MYNN-Kz	16.4	19.0	−0.55	0.69	−0.26	0.58
Urban	25	31.0	R-YSU	31.2	20.5	−0.13	0.53	0.15	0.62
			R-MYNN	32.5	20.7	−0.08	0.52	0.20	0.63
			UC-YSU	22.4	19.3	−0.40	0.62	−0.16	0.54
			UC-MYNN	25.4	19.2	−0.29	0.58	−0.05	0.55
			UC-YSU-Kz	21.3	19.4	−0.45	0.64	−0.20	0.54
			UC-MYNN-Kz	18.1	20.4	−0.56	0.69	−0.30	0.54
Suburban	5	21.7	R-YSU	18.5	15.2	−0.29	0.58	−0.04	0.57
			R-MYNN	18.8	15.0	−0.26	0.55	−0.02	0.56
			UC-YSU	12.6	15.8	−0.56	0.70	−0.32	0.53
			UC-MYNN	14.7	14.9	−0.43	0.62	−0.22	0.51
			UC-YSU-Kz	12.0	15.9	−0.60	0.72	−0.36	0.53
			UC-MYNN-Kz	11.3	16.0	−0.63	0.72	−0.39	0.52
Rural	2	9.8	R-YSU	8.3	8.2	−0.16	0.65	0.57	1.12
			R-MYNN	7.8	8.3	−0.18	0.61	0.41	0.97
			UC-YSU	7.3	7.8	−0.22	0.66	0.46	1.07
			UC-MYNN	6.9	7.7	−0.24	0.63	0.34	0.96
			UC-YSU-Kz	5.9	8.4	−0.41	0.73	0.30	1.07
			UC-MYNN-Kz	7.8	8.2	−0.22	0.71	0.56	1.19

[a], [b], [c]: for the detailed caption of the table, see Table 4a.

similar NO_2 concentration at both Eiffel and Paris-7. Both simulations model well the observed mean NO_2 concentration at Paris-7. However, NO_2 is strongly under-estimated at Eiffel. The observed NO_2 concentration at Eiffel is about half that at Paris-7, while the modeled NO_2 concentration at Eiffel is only 17–19% of the modeled NO_2 at Paris-7, suggesting that vertical mixing is under-estimated in the Reference simulations. The ratio of NO_2 concentrations at Eiffel and Paris-7 is improved using the UCM and the Corine land-use. However, the NO_2 concentrations are still under-estimated at both Eiffel and Paris-7.

Because O_3 concentration is not available at Paris-7, a comparison of the O_3 concentration at Eiffel to the concentration averaged over the BDQA urban stations (see Table 4c) may be useful. The Reference simulations over-estimate the concentrations of O_3 at Eiffel. The observed concentration of O_3 at Eiffel is similar to the concentration averaged over the BDQA urban stations. However, the modeled concentration at Eiffel is significantly higher than the concentration averaged over the urban stations. Similarly to the increase of O_3 with the UCM-Corine simulations at BDQA ground stations (see Section 3.1), concentrations of O_3 are slightly lower

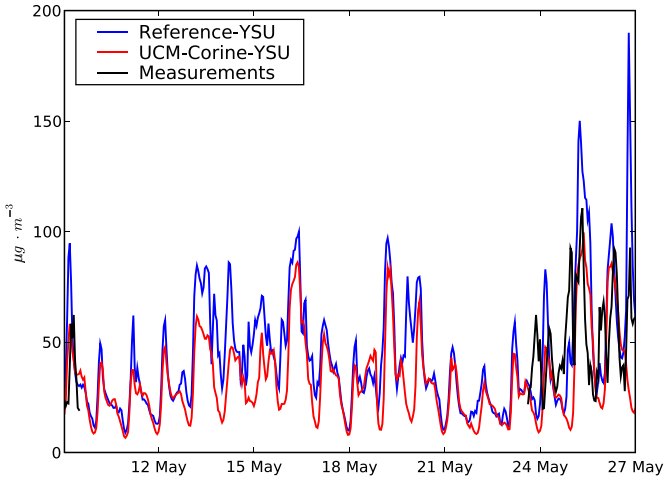

Fig. 4. Temporal variations of observed and modeled NO_2 concentrations from 9 to 27 May at an urban station in Paris, Les Halles (48.86° N, 2.35° E).

than those of the Reference simulations when the UCM and the Corine land-use are used because of the increase in NO_2 concentrations. In the UCM-Corine simulations, the O_3 concentration at Eiffel is closer to the O_3 concentration averaged over surface stations, suggesting that vertical mixing is better simulated even though it may still be under-estimated. This conclusion is in agreement with Kim et al. (2013) who found that the UCM and the Corine land-use improved the modeling of the PBL height over Greater Paris.

3.3. Comparisons to lidar measurements

The PM_{10} vertical distribution was measured using a GBML during the air quality observation campaign, LIdar pour la Surveillance de l'AIR (LISAIR) in Greater Paris from 24 to 27 May 2005 (Raut and Chazette, 2009). Observations of the aerosol extinction coefficients profiles by the GBML were performed to retrieve the vertical distribution of PM_{10}. Observations performed on 24 and 25 May at nighttime illustrate the presence of an inversion layer trapping pollutants at low altitudes and a residual layer at higher altitudes. PM_{10} gradients between the suburbs of Paris (Palaiseau) and Paris center (Les Halles) were observed, and observations along main roads and the beltway of Paris were carried out. The routes followed by the automobile embarking the lidar are presented in Fig. 5. Details on the GBML measurements can be found in Raut and Chazette (2009). PM_{10} concentrations are deduced from the lidar signal following Raut and Chazette (2009) by taking into account influence of humidity on extinction coefficients. A discussion on the influence of humidity and comparisons of extinction coefficients are presented in A. In the following, we compare the vertical concentrations of PM_{10} retrieved by the lidar to the modeled concentrations.

3.3.1. Comparison at Les Halles (urban station) before traffic

Fig. 6a presents the vertical distribution of PM_{10} at Les Halles, Paris center on 24 May at 0357 UTC. The Reference simulations over-estimate surface PM_{10} concentration: 9 μg m^{-3} from the BDQA database vs 37 μg m^{-3} (YSU) and 36 μg m^{-3} (MYNN). Because vertical mixing is greater (see Section 3.1.4) and K_z is higher in the PBL in the UCM-Corine simulations (see Fig. 6b), the over-estimations are reduced in the UCM-Corine simulations: 26 μg m^{-3} with YSU scheme and 24 μg m^{-3} with the MYNN scheme. PM_{10} is over-estimated in the nocturnal boundary layer in all the simulations while PM_{10} is under-estimated in the residual layer and over-estimated above. PM_{10} concentrations in the Reference-YSU simulation are higher than those in the Reference-MYNN simulation between 0.2 and 0.7 km, because the PBL height computed in the WRF simulation for the Reference-MYNN simulation is lower (169 m) than that for the Reference-YSU simulation (690 m). As shown in Section 3.1.4 for surface concentrations, in the first 200 m, differences in PM_{10} concentrations induced by using the UCM and the Corine land-use are larger than differences induced by using different PBL schemes. However, the opposite is observed between 200 m and below the residual layer. Although PM_{10} concentrations tend to be under-estimated in the residual layer, the Reference-MYNN simulation manages to reproduce the observed residual layer between 0.8 and 1.1 km. However, it under-estimates the PM_{10} concentrations between 1.1 and 1.5 km, which may be due to regional transport as suggested by Raut and Chazette (2009).

Fig. 6e presents the vertical distribution of PM_{10} at Les Halles, Paris center on 25 May at 0357 UTC. Comparisons of Fig. 6a and e allow one to compare the PM_{10} vertical distributions at the same place and same time on different days (i.e., different weather conditions). Less developed PBL on 25 May results in higher surface PM_{10} concentrations (25 μg m^{-3}) than on 24 May (9 μg m^{-3}). While the Reference simulations over-estimate surface PM_{10} concentration: 76 μg m^{-3} with the YSU scheme and 69 μg m^{-3} with the

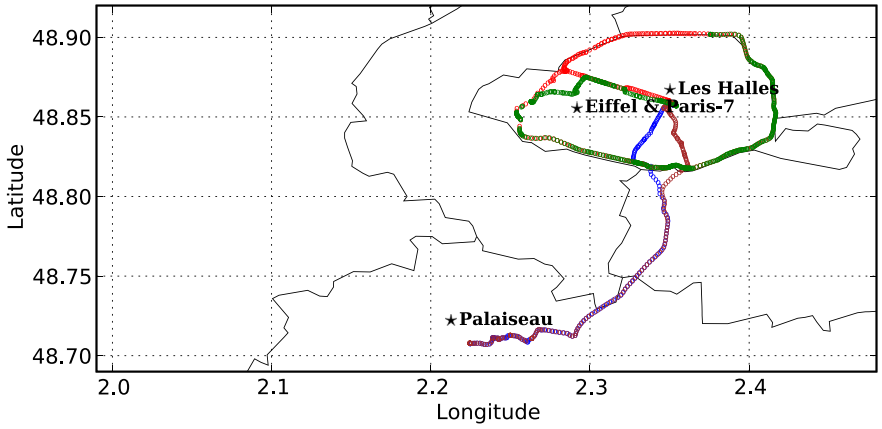

Fig. 5. Locations of observation stations and route taken for the measurements of the GBML. Blue and brown marks show the route for the measurements from the suburbs of Paris (Palaiseau) to Paris center (Les Halles) on 24 and 25 May, respectively. Red marks are for the measurements on the beltway of Paris before rush-hour and green marks are for the measurements on the beltway during rush-hour on 25 May. The black lines show the geographical boundary of the administrative departments. (For interpretation of the references to colour in this figure legend, the reader is referred to the web version of this article.)

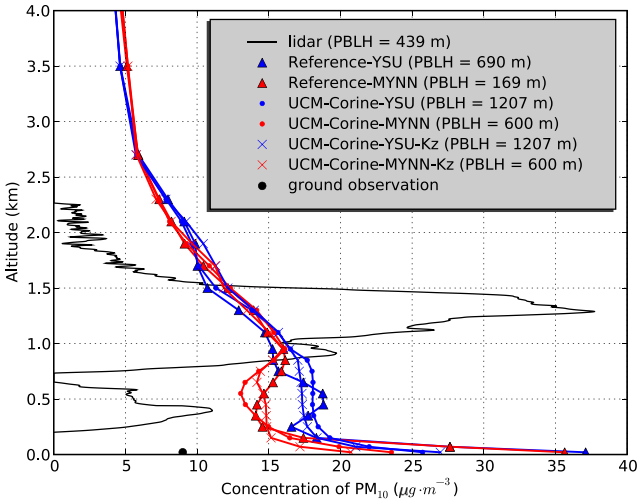

(a) PM_{10} on 24 May, 0357 UTC at Paris, Les Halles

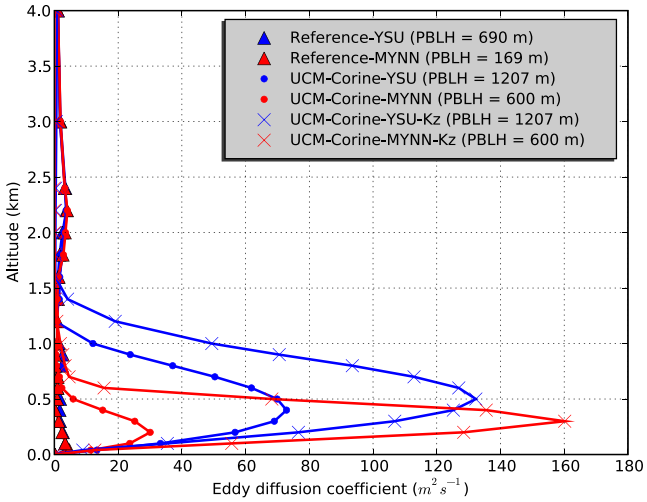

(b) K_z on 24 May, 0357 UTC at Paris, Les Halles

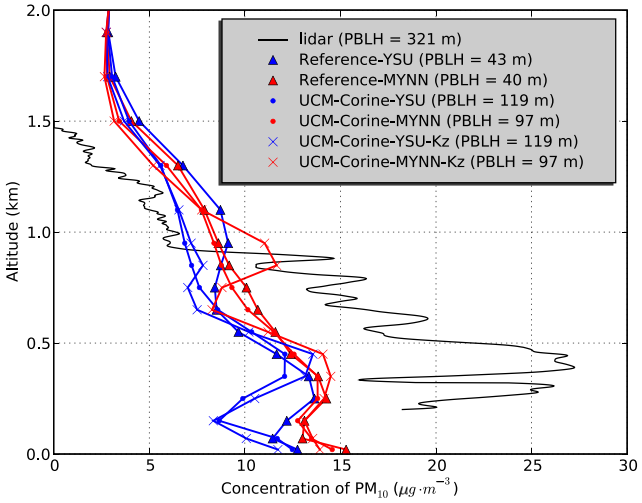

(c) PM_{10} on 25 May, 0309 UTC at Palaiseau

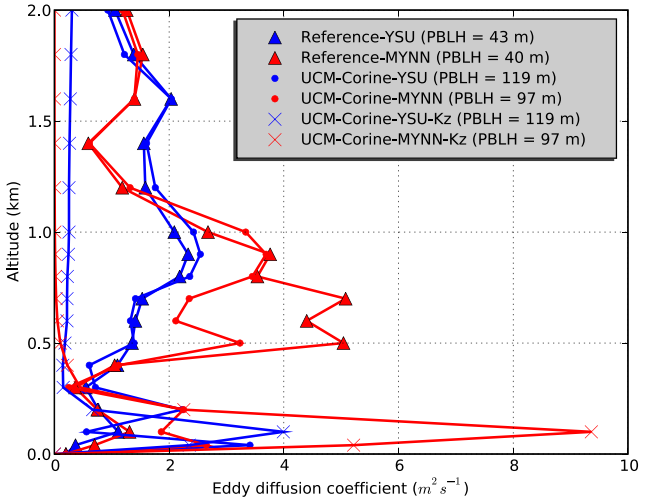

(d) K_z on 25 May, 0309 UTC at Palaiseau

Fig. 6. Observed and modeled PM_{10} vertical distributions at Les Halles (48.86° N, 2.35° E) and Palaiseau (48.71° N, 2.22° E) are compared in the left column. PBLH are planetary boundary layer height estimated by the lidar or diagnosed in the simulations. Black circles in (a), (e) and (g) represent observed PM_{10} at the surface stations. In the right column, modeled K_z are shown.

MYNN scheme, the results obtained in the UCM-Corine simulations agree qualitatively well with the observed surface PM_{10}: 31 μg m^{-3} with the YSU scheme and 37 μg m^{-3} with the MYNN scheme. The PBL height is under-estimated in all simulations (264 m maximum for the UCM-Corine-YSU simulation against 477 m from the measurements), leading to an under-estimation of PM_{10} between 0.2 and 0.5 km above the modeled PBL height. As on 24 May, PM_{10} in the residual layer tends to be under-estimated but over-estimated above.

3.3.2. *Comparison at Palaiseau (suburban station) before traffic*

Fig. 6c presents the vertical distribution of PM_{10} at Palaiseau, a suburb of Paris on 25 May at 0309 UTC. PM_{10} is under-estimated in all the simulations below 0.9 km and over-estimated above 0.9 km. The PBL height is under-estimated in all simulations (119 m maximum for the UCM-Corine-YSU simulation against 321 m from the measurements). The Reference-YSU and Reference-MYNN simulations reproduce the residual layer between 0.2 and 0.6 km but underestimate concentrations. The lower concentrations in the residual layers are partly linked to uncertainties in local PM_{10} emissions, mostly in dust resuspension. Amato et al. (2009) presented a model of road dust resuspension in Barcelona. The model calculates a percentage of the total traffic emissions for the road dust resuspension. This percentage is 37% for PM_{10}. In general, meteorological conditions in Paris differ to those in Barcelona. However, the weather conditions (clear sky and weak wind) during this period were favorable to dust resuspension with low precipitation. Therefore, although results for Barcelona should not be used for Paris, they may be adequate to Paris for this particular dry period. If this percentage is applied to the traffic emissions from the AIRPARIF inventory in Table 1, PM_{10} emissions by road transport would increase from 7998 ton yr^{-1} to 12,695 ton yr^{-1} including 4697 ton yr^{-1} of dust resuspension. This amount would account for 17.5% of total PM_{10} emissions, in agreement with the estimation

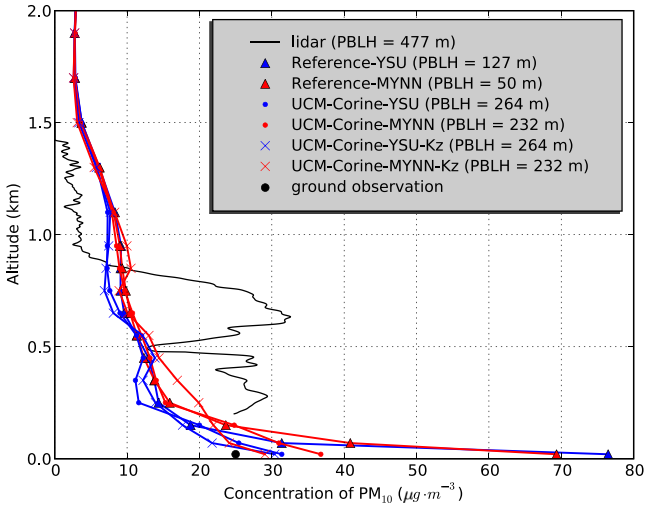

(e) PM_{10} on 25 May, 0357 UTC at Paris, Les Halles

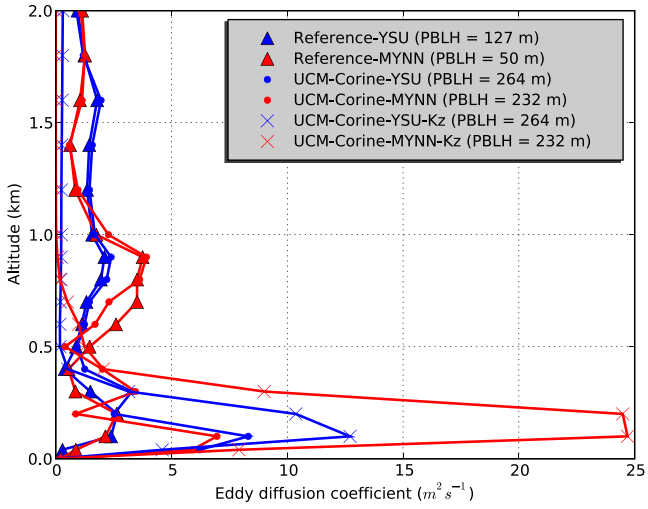

(f) K_z on 25 May, 0357 UTC at Paris, Les Halles

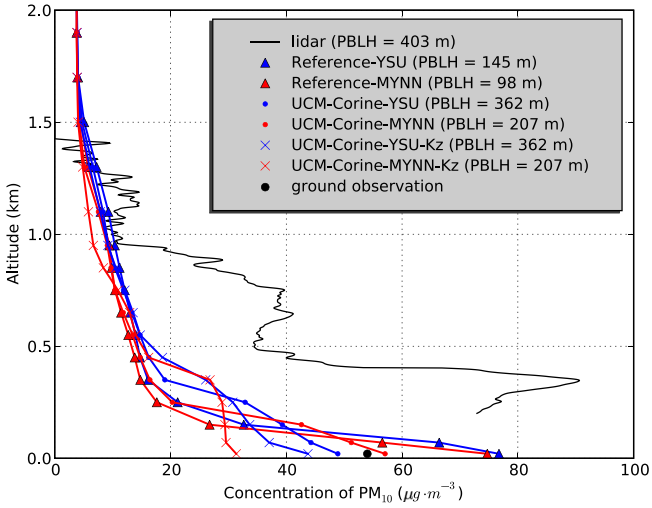

(g) PM_{10} on 25 May, 0755 UTC at Paris, Les Halles

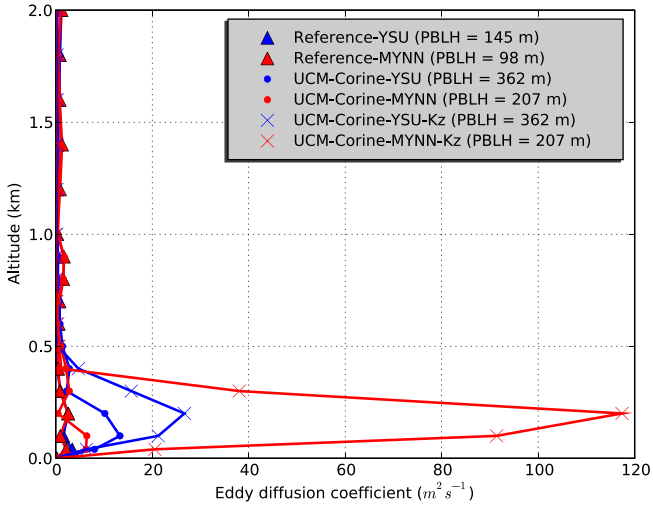

(h) K_z on 25 May, 0755 UTC at Paris, Les Halles

Fig. 6. (*continued*).

(17%) of Amato et al. (2009).

3.3.3. *Influence of traffic*

To study the influence of automobile traffic on PM_{10} concentrations, measurements performed at the same place (Les Halles) at 0357 UTC (before rush hour) and at 0755 UTC (during rush hour) are compared in Fig. 6e and g. Surface PM_{10} concentrations from the BDQA database increase from 25 μg m^{-3} at 0357 UTC to 54 μg m^{-3} at 0755 UTC. At 0755 UTC, surface PM_{10} concentrations are over-estimated in the Reference simulations: 77 μg m^{-3} with the YSU scheme and 75 μg m^{-3} with the MYNN scheme, but they are well modeled in the UCM-Corine simulations: 49 μg m^{-3} with the YSU scheme and 57 μg m^{-3} with the MYNN scheme. Lidar measurements show a large increase of PM_{10} concentrations in the PBL, from concentrations lower than 30 μg m^{-3} at 0357 UTC to concentrations higher than 90 μg m^{-3} at 0755 UTC. PM_{10} concentrations at 0755 UTC are more under-estimated in the PBL than at 0357 UTC. This suggests that the non-inclusion of dust resuspension in the emission inventory is particularly significant under conditions of high traffic. PM_{10} concentrations are under-estimated in the PBL, even though the PBL height is under-estimated in all simulations

Table 5
Comparison of modeled concentrations to observations averaged from 9 to 27 May for 11 urban stations of the BDQA database (μg m^{-3}).

	Whole day	Daytime	Nighttime
Observation	17.8	19.4	16.1
Reference-YSU	19.2	19.0	19.4
Reference-MYNN	20.3	19.6	21.1
UCM-Corine-YSU	15.9	16.9	14.9
UCM-Corine-MYNN	17.5	18.0	16.9
UCM-Corine-YSU-Kz	15.4	16.0	14.7
UCM-Corine-MYNN-Kz	15.0	14.8	15.2

Table 6
Comparison of modeled concentrations to observations at the Eiffel Tower and Paris-7 stations.

	Stations	Observed mean[a] (μg m^{-3})	Model	Modeled mean[a] (μg m^{-3})	RMSE (μg m^{-3})	MFB	MFE	MNB	MNGE
O_3	Eiffel	55.9	Reference-YSU	77.4	31.3	0.40	0.44	0.93	0.97
			Reference-MYNN	77.9	32.2	0.40	0.45	0.95	0.99
			UCM-Corine-YSU	76.0	30.0	0.37	0.44	0.85	0.91
			UCM-Corine-MYNN	74.5	29.2	0.36	0.43	0.82	0.87
			UCM-Corine-YSU-Kz	76.5	30.9	0.38	0.45	0.88	0.95
			UCM-Corine-MYNN-Kz	74.5	30.0	0.35	0.43	0.85	0.92
NO_2	Eiffel	22.0	Reference-YSU	8.1	19.8	−0.83	0.88	−0.50	0.61
			Reference-MYNN	7.8	20.4	−0.89	0.94	−0.53	0.63
			UCM-Corine-YSU	11.2	16.4	−0.58	0.67	−0.36	0.51
			UCM-Corine-MYNN	11.7	16.7	−0.53	0.63	−0.32	0.49
			UCM-Corine-YSU-Kz	10.4	17.1	−0.66	0.75	−0.41	0.56
			UCM-Corine-MYNN-Kz	11.7	16.3	−0.56	0.67	−0.33	0.52
	Paris-7	43.8	Reference-YSU	43.4	21.5	−0.21	0.41	−0.11	0.34
			Reference-MYNN	45.2	22.6	−0.16	0.35	−0.07	0.31
			UCM-Corine-YSU	32.3	22.6	−0.54	0.58	−0.37	0.41
			UCM-Corine-MYNN	35.8	22.5	−0.47	0.52	−0.31	0.37
			UCM-Corine-YSU-Kz	31.2	22.9	−0.36	0.49	−0.22	0.40
			UCM-Corine-MYNN-Kz	25.5	26.0	−0.53	0.60	−0.35	0.45

[a] Mean concentrations from 9 to 27 May.

(362 m maximum in the UCM-Corine-YSU simulation against 403 m from the measurement).

3.3.4. Impact of the eddy–diffusion coefficient

Fig. 6b, d, f and h compare K_z on 24 May 0357 UTC at Les Halles, on 25 May 0309 UTC at Palaiseau, on 25 May 0357 UTC and 0755 UTC at Les Halles respectively. At all places and times, the K_z extracted from outputs of the WRF simulation with the MYNN scheme is significantly different from the preprocessed K_z in Polyphemus. The differences are lower if the YSU scheme is used rather than the MYNN scheme in the WRF simulation, because the parameterization of K_z in the YSU scheme is based on the method of Troen and Mahrt.

As expected, the influence of using K_z extracted from outputs of the WRF simulation on the PM_{10} vertical distribution is higher with the MYNN scheme than with the YSU scheme, suggesting that the impact of preprocessed K_z in Polyphemus is low when the YSU scheme is used in the WRF simulation. However, the differences of PM_{10} concentrations between the UCM-Corine-MYNN and UCM-Corine-MYNN-Kz simulations are higher than those between the UCM-Corine-YSU and UCM-Corine-MYNN simulations on 25 May 0357 UTC and on 25 May 0755 UTC at Les Halles.

Despite the higher K_z values in the UCM-Corine-MYNN-Kz and UCM-Corine-YSU-Kz simulations than in the UCM-Corine-MYNN and UCM-Corine-YSU simulations, PM_{10} still tends to be underestimated in the residual layers.

4. Sensitivities of wind, temperature, humidity and K_z on strongly urbanized regions

In the previous sections, we analysed the results by assuming that using different PBL schemes and/or the UCM and the Corine land-use mostly impacts vertical mixing and the PBL height. However, in addition to vertical mixing, it may also impact other meteorological parameters, such as wind, temperature and humidity.

To estimate which meteorological fields mostly impact the PM_{10} vertical distribution when using different PBL schemes, and/or the UCM and the Corine land-use, we conducted additional simulations with modified meteorological fields. For sensitivity to PBL schemes, the Reference-MYNN simulation was repeated with some modified meteorological variables (see Table 7 for a list of simulations). In these sensitivity simulations, we replaced a meteorological variable with the variable modeled using the YSU scheme. The examined variables are wind fields (speed and direction), temperature, humidity and K_z. We compare the differences in vertical distribution of PM_{10} concentrations between the sensitivity simulations and the Reference-MYNN simulation over a sub-domain strongly urbanized for most grid cells, the Greater Paris (see Fig. 2 for the domain). The sub-domain represents an urban region: the urban fraction of the land-use data is larger than 0.9. As this sub-domain is quite homogeneous, influence of domain-averaging may be low. Fig. 7a–c present the differences for wind fields, humidity and K_z respectively. The impact of using wind fields modeled by the YSU scheme is significant from the surface to about 3 km of altitude. The maximum domain-averaged difference is about 8% at about 2 km of altitude. The differences between the Reference-MYNN simulation and the Reference-MYNN-Wind simulation are important compared to the total differences between the Reference-YSU and Reference-MYNN simulations presented in Fig. 8d (50% of the total difference at the surface). The impact of using temperature modeled by the YSU scheme is lower than that of wind fields. The domain-averaged difference is lower than 3% and negligible above 1 km of altitude (not shown). The impact of using humidity modeled by the YSU scheme is significant between 1 and 3 km of altitude with a maximum of 10% at 1.7 km. Below 1.5 km of altitude, the impact of K_z is significant and the maximum domain-averaged difference is about 5%.

Table 7
Characteristics of the simulations with modified meteorological fields.

Name	PBL scheme	Using UCM	Land-use data	Modified meteorological field
Reference-MYNN-Wind	MYNN	No	USGS	Wind fields from YSU
Reference-MYNN-Humidity	MYNN	No	USGS	Humidity from YSU
Reference-MYNN-Mixing	MYNN	No	USGS	PBLH and K_z from YSU
UCM-Corine-YSU-Wind	YSU	Yes	Corine	Wind fields without UCM/Corine
UCM-Corine-YSU-Humidity	YSU	Yes	Corine	Humidity without UCM/Corine
UCM-Corine-YSU-Mixing	YSU	Yes	Corine	PBLH and K_z without UCM/Corine

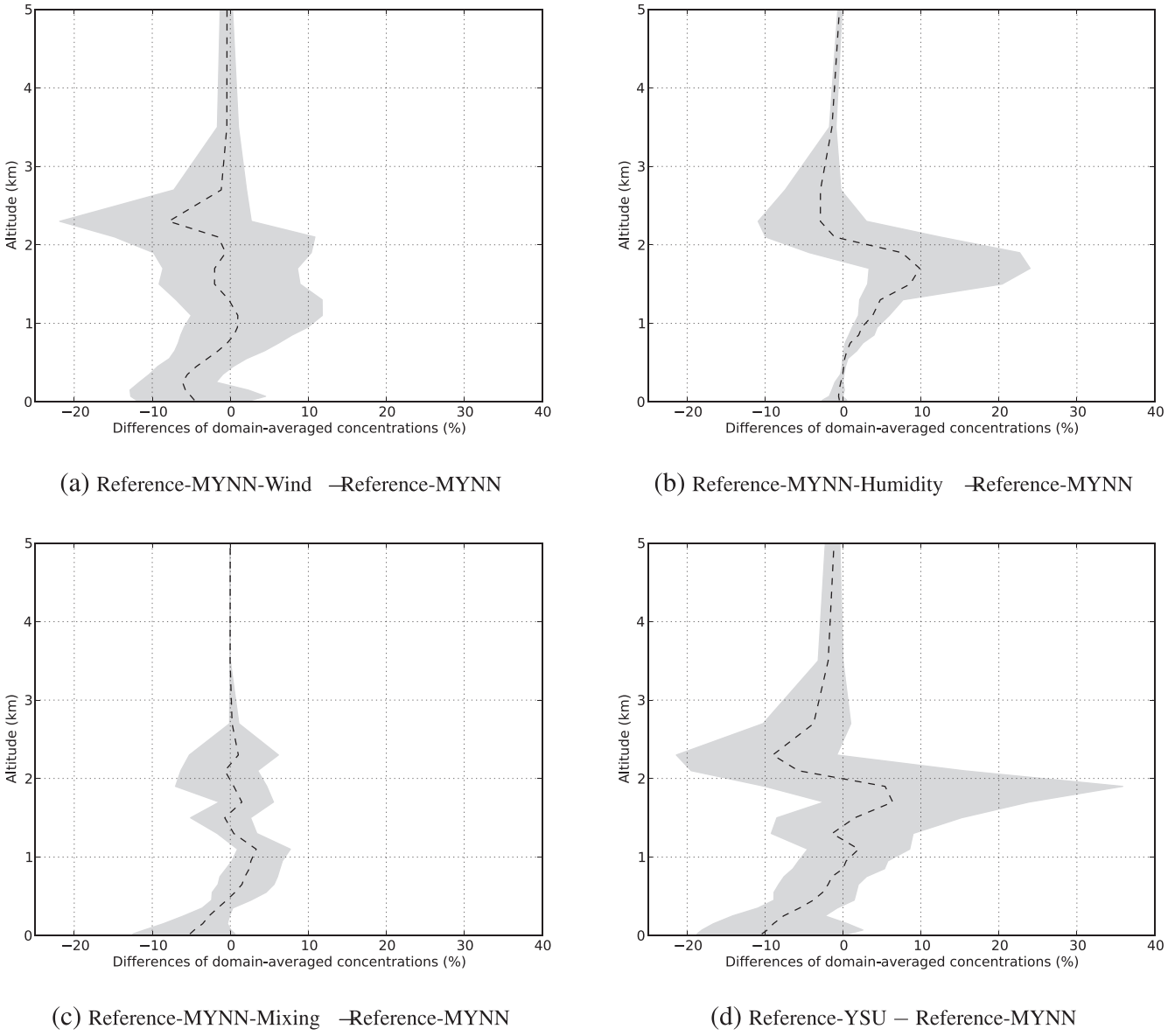

Fig. 7. Differences in domain-averaged concentrations of modeled PM_{10} between the Reference-MYNN simulation and sensitivity simulations for 4 days between 9 and 12 May 2005. The dashed lines correspond to domain-averaged concentrations and the shaded regions show the range of local values. The simulations are listed in Table 7.

For sensitivity to the UCM and the Corine land-use, the UCM-Corine-YSU simulation was used as the reference simulation and sensitivity simulations were conducted (see Table 7 for a list of simulations). We replaced a meteorological variable with the variable modeled without the UCM and the Corine land-use. We compare the differences in vertical distribution of PM_{10} concentrations between the sensitivity simulations and the UCM-Corine-YSU simulation. Fig. 8a–c present the differences for wind fields, humidity and K_z respectively. For the sensitivity to the UCM, the impacts of temperature, wind fields and humidity are lower than for the sensitivity to the PBL schemes. The maximum domain-averaged differences are 4% and 3% for wind fields and humidity, respectively. However, the impact of K_z (about 5%) is similar to that for the sensitivity to the PBL schemes from the surface to 1.5 km of altitude. Fig. 8d shows that most of differences below 1.5 km of altitude between the Reference-YSU and UCM-Corine-YSU simulations is caused by the increase of modeled PBL height and K_z with the UCM and the Corine land-use.

5. Conclusions

Sensitivities of the vertical dispersion of pollutants to different meteorological and physical parameterizations (PBL schemes, UCM and K_z) were studied using off-line meteorology (WRF) and chemistry-transport (Polair3D/Polyphemus) models. Two different PBL schemes were used (the MYNN and YSU schemes) and the UCM was turned on and off.

Comparisons at surface stations (BDQA network) and at an upper air station (the Eiffel Tower) show that simulations with the UCM and the Corine land-use globally perform better. At surface stations, $PM_{2.5}$ is better modeled with the UCM, as well as PM_{10} to a lesser extent. The impacts of the UCM on PM_{10} are greater at urban stations than at suburban and rural stations. However, for O_3, using the UCM does not improve the modeled surface concentrations. The UCM leads to an increase of mixing and therefore to lower NO_2 concentrations and higher O_3 near the surface. As O_3 concentrations tend to be slightly over-estimated at surface stations, using the UCM increases this over-estimation. However, at the upper air

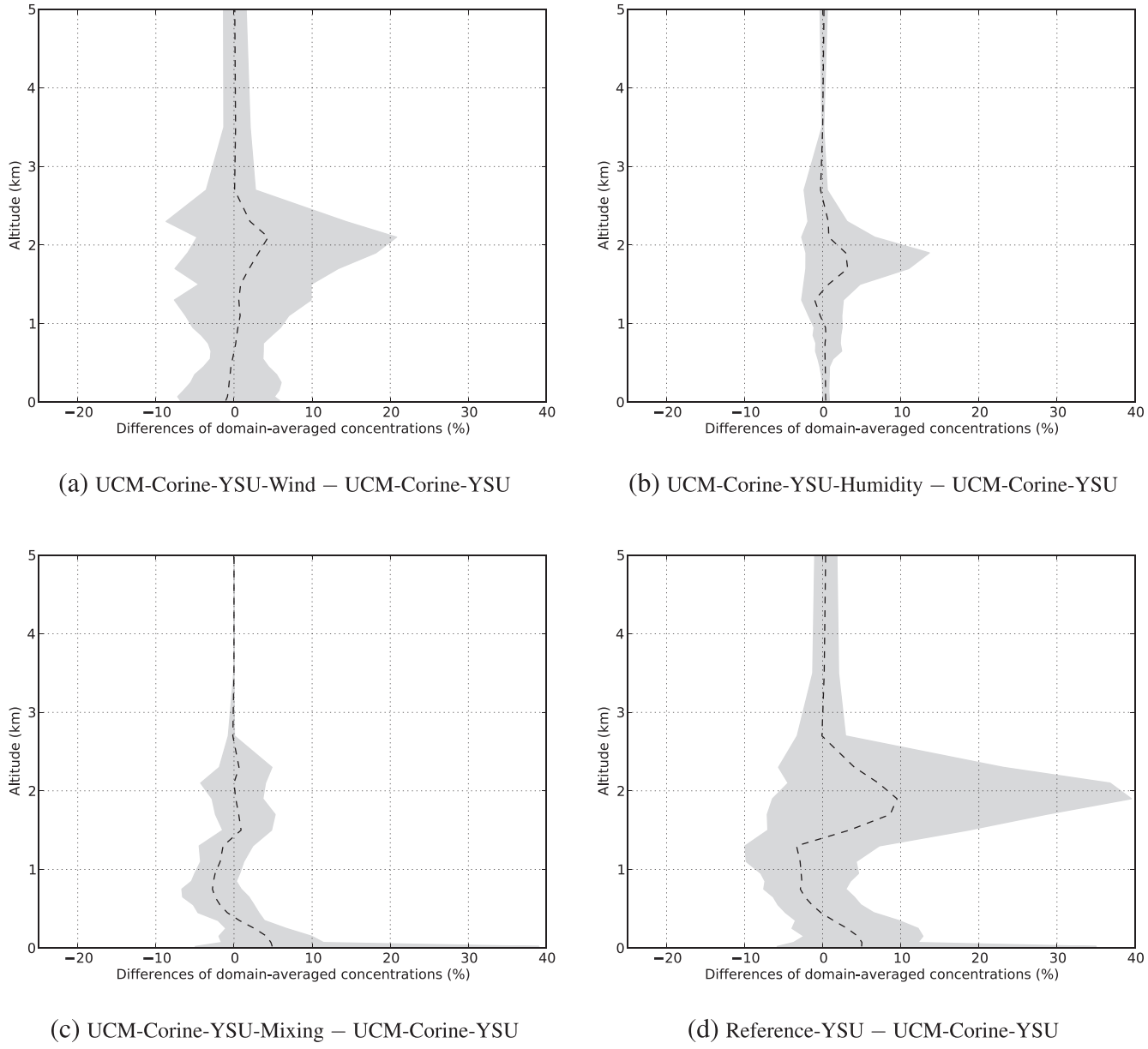

Fig. 8. Differences in domain-averaged concentrations of modeled PM_{10} between the UCM-Corine-YSU simulation and sensitivity simulations for 4 days between 9 and 12 May 2005. The dashed lines correspond to domain-averaged concentrations and the shaded regions show the range of local values. The simulations are listed in Table 7.

station, NO_2 and O_3 are both better modeled using the UCM, because the UCM better represents vertical mixing, which was under-estimated. Higher surface concentrations are obtained for PM_{10}, $PM_{2.5}$ and NO_2 with the MYNN scheme than the YSU scheme, suggesting weaker vertical mixing in the MYNN scheme. Differences between simulations using different PBL schemes are lower than differences between simulations with and without the UCM and the Corine land-use.

Concerning the comparisons of the modeled PM_{10} vertical distributions to the distributions obtained from lidar measurements, PM_{10} is under-estimated in the PBL on 25 May but over-estimated on 24 May during nighttime at Paris center (Les Halles). The over-estimation of PM_{10} in the PBL on 24 May is greater with the YSU scheme than the MYNN scheme because lower PBL height with the MYNN scheme leads to weaker vertical mixing. Using the UCM and the Corine land-use leads to stronger vertical mixing for both PBL schemes at Les Halles. PM_{10} concentrations tend to be under-estimated in the residual layer while they tend to be over-estimated over the residual layer. The under-estimation of PM_{10} concentrations is linked to uncertainties in PM_{10} emissions, in particular, road dust resuspension, and to an over-estimation of vertical mixing during nighttime at high altitudes.

Using two different PBL schemes in WRF leads not only to different vertical mixing parameters (K_z and PBL height), but also to different horizontal winds and humidities. They all influence the PM_{10} distribution computed by the CTM. The difference caused by wind fields accounts for 50% of the total difference at the surface. Using the UCM and the Corine land-use affects PM_{10} vertical distribution by the increase of modeled PBL height and K_z below 1.5 km of altitude and by the differences in wind fields and humidity aloft.

The results of this work imply that the model performance for the PM_{10} vertical dispersion is improved using the UCM and the Corine land-use over urbanized areas. In particular, the vertical

mixing strength in the nocturnal boundary layer is significantly improved over suburban and urban regions. However, further improvements are necessary in modeling diurnal variation of pollutant concentrations using the UCM and the Corine land-use. The diagnosis of nocturnal boundary layer heights still needs to be improved, particularly over suburban regions. In this study, only one urban category of land-use data was used. More categories of urban land-use data would be required to take into account more accurate geometric and thermal characteristics in the WRF model.

Acknowledgements

The authors acknowledge AIRPARIF for providing ozone and PM measurement data. Thanks are due to our colleague, Christian Seigneur for helpful discussions and advices on the manuscript.

Appendix A. Comparison of extinction coefficients

In the comparisons of the PM_{10} vertical distributions in Section 3.3, PM_{10} concentrations were derived from lidar measurements by Raut and Chazette (2009) using an empirical optical-to-mass relationship between dry PM_{10} concentrations in the PBL and dry extinction coefficients. This relationship was established from nephelometer and TEOM (Tapered element oscillating microbalance) in-situ measurements (Raut and Chazette, 2009). However, depending on the relative humidity (RH) and their chemical composition, particles may absorb water vapor. The extinction coefficient obtained from lidar measurements is a wet one, that is, it takes into account all chemical components of particles including water. This wet extinction coefficient was used instead of the dry one to derive PM_{10} concentrations.

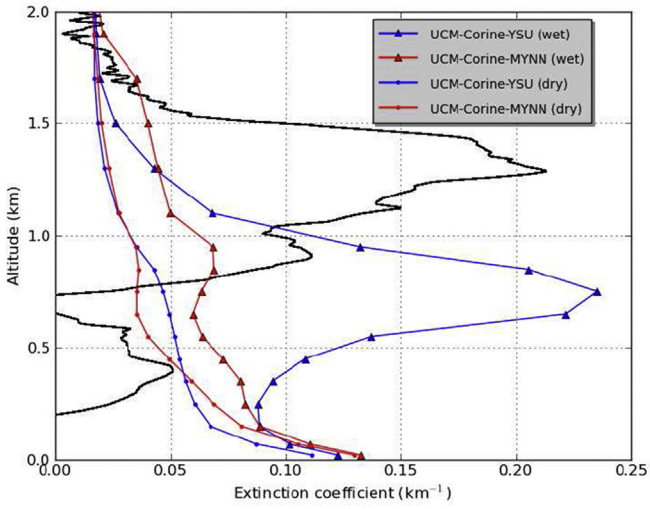

(a) α (km^{-1}) on 24 May, 0357 UTC at Paris, Les Halles

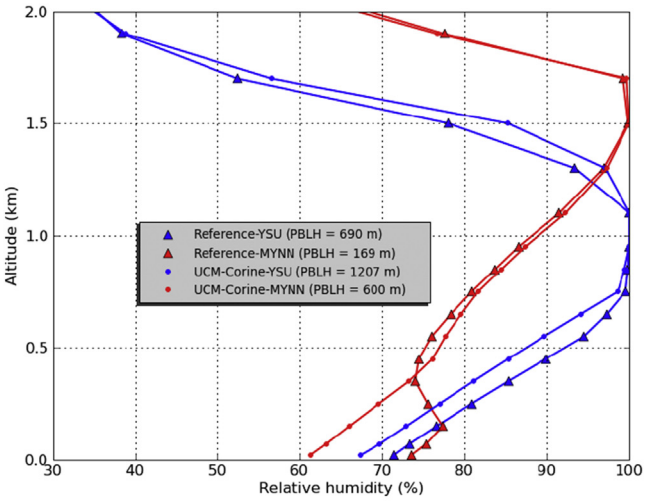

(b) RH (%) on 24 May, 0357 UTC at Paris, Les Halles

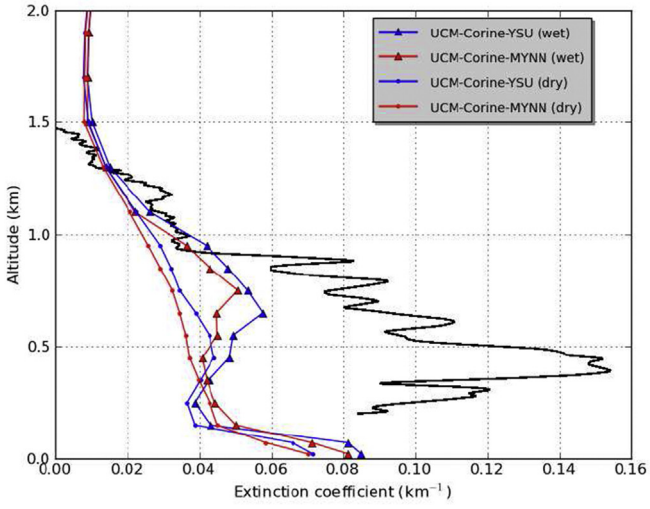

(c) α (km^{-1}) on 25 May, 0309 UTC at Palaiseau

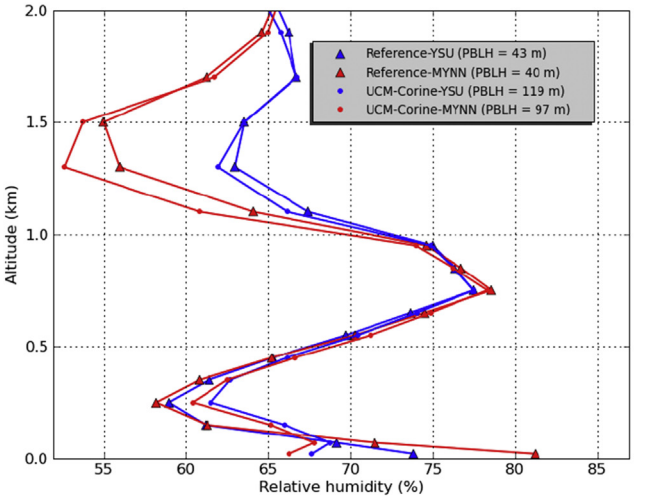

(d) RH (%) on 25 May, 0309 UTC at Palaiseau

Fig. A1. Observed and modeled extinction coefficients (α) at Les Halles (48.86° N, 2.35° E) and Palaiseau (48.71° N, 2.22° E) are compared in the left column. Modeled relative humidities (RH) are shown in the right column.

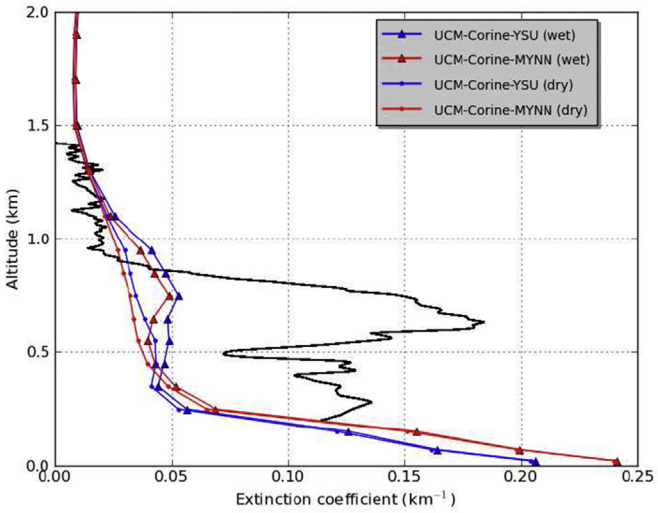

(e) α (km^{-1}) on 25 May, 0357 UTC at Paris, Les Halles

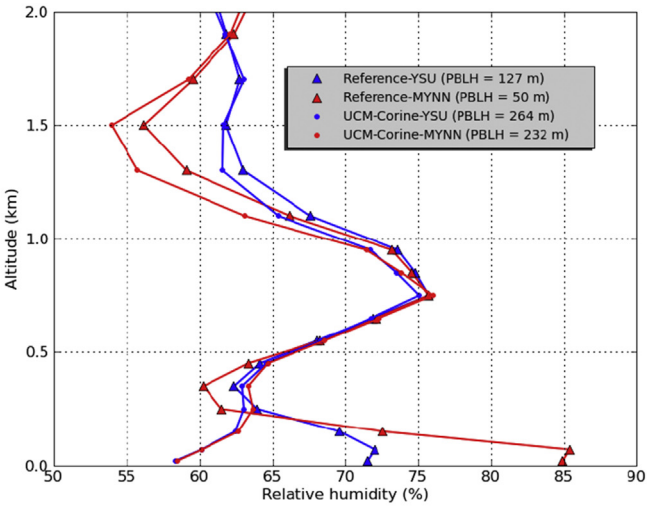

(f) RH (%) on 25 May, 0357 UTC at Paris, Les Halles

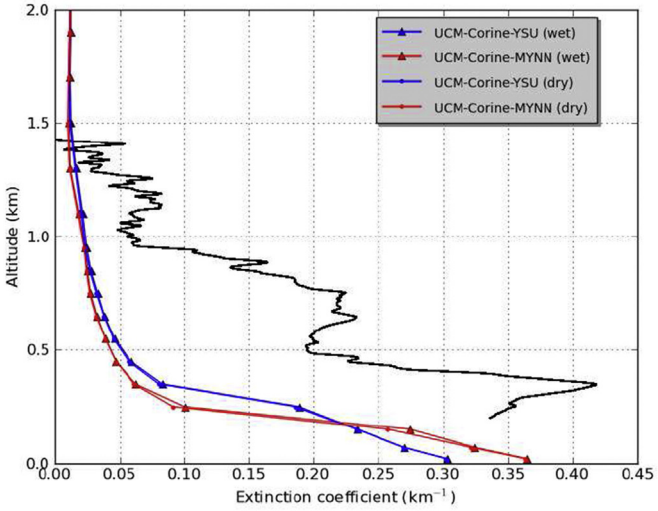

(g) α (km^{-1}) on 25 May, 0755 UTC at Paris, Les Halles

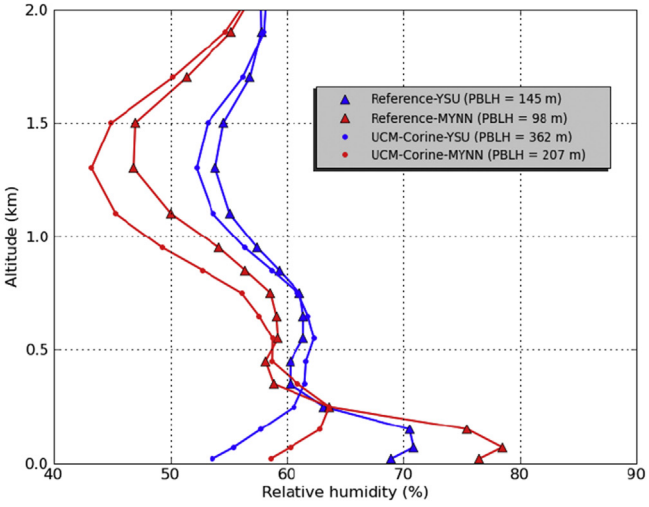

(h) RH (%) on 25 May, 0755 UTC at Paris, Les Halles

Fig. A1. (*continued*).

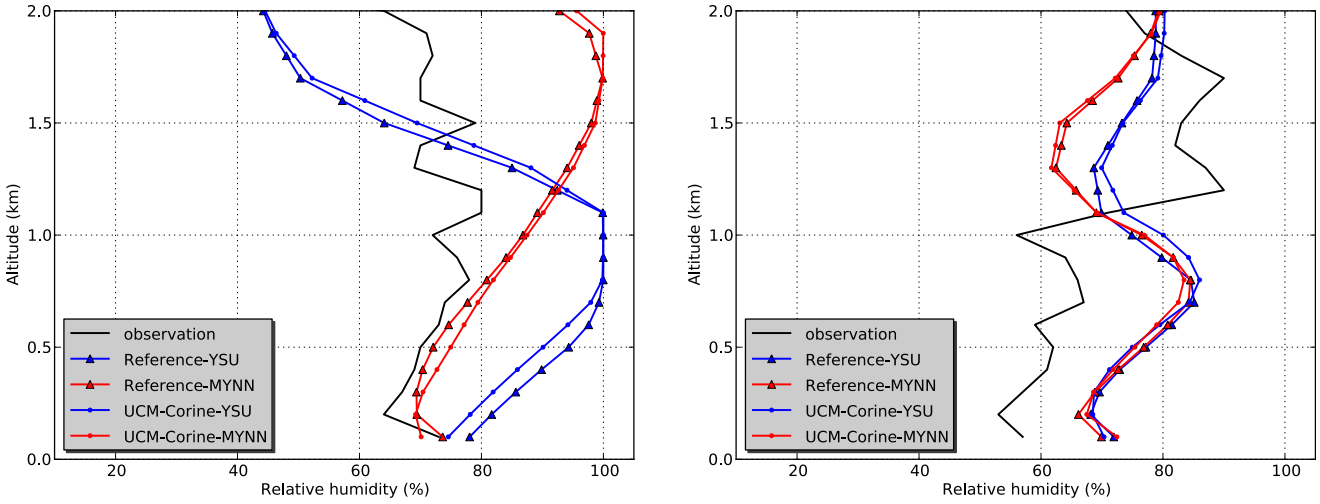

(a) RH on 23 May 2305 UTC at Trappes (b) RH on 24 May 2330 UTC at Trappes

Fig. A2. Vertical profiles of observed and modeled RH. Observations are performed using the radiosonde at Trappes (48.78° N, 2.00° E).

To assess the role of water in the comparisons of the PM_{10} vertical distributions, wet (α_{wet}) and dry (α_{dry}) extinction coefficients computed from the simulations were compared to each other and to extinction coefficients obtained from lidar measurements in Fig. A1. The computation of the α_{wet} and α_{dry} from the simulations was done using a postprocessing tool of Polyphemus (Real and Sartelet, 2011).

The comparison of α_{wet} to observation (see Fig. A1) exhibits similar patterns to the comparison of PM_{10} concentrations (see Fig. 6). On 24 May 0357 UTC at Les Halles, they are slightly over-estimated in the PBL below 0.7 km and under-estimated above 0.8 km. They are under-estimated on 25 May in both the PBL and the residual layer.

The differences between the simulated α_{dry} and α_{wet} are not significant for the three profiles of 25 May while they are important on 24 May 0357 UTC at Les Halles, especially between 0.5 km and 1 km height when the YSU scheme is used to compute meteorological fields (Fig. A1a). The low differences between α_{dry} and α_{wet} are due to relatively low RH because the low RH can be lower than deliquescence RH.

The higher differences between α_{dry} and α_{wet} on 24 May 0357 UTC are a consequence of high RH. When the YSU scheme is used, RH reaches a value of almost 100% in the residual layer (see Fig. A1b). However, this high RH is not observed by the radiosonde at Trappes on 23 May 2305 UTC (see Fig. A2a). The station at Trappes is 27 km southwest of Paris and is in an urban environment. The RH are over-estimated below 1 km height, suggesting an over-estimation of α_{wet}. However the over-estimation of RH on 24 May 2330 UTC (see Fig. A2b) did not bring an over-estimation of α_{wet} below 1 km height. It implies uncertainties about the influences of RH on α_{wet}.

In conclusion, α_{wet} should not be significantly different from α_{dry} for the vertical profiles of 24 and 25 May, and the empirical optical-to-mass relationship used to derive PM_{10} concentrations from extinction coefficients may be used.

References

ADEME, 2002. Classification and Criteria for Setting up Air-quality Monitoring Stations. Available at: http://www2.ademe.fr/servlet/getBin?name=07FDD830B431AE40B6CB835B250DD21F1137074135479.pdf (accessed 11.04.14.).

AIRPARIF, 2004. Évaluation de la qualité de l'air en Île-de-France à l'échéance 2010 et impact du Plan de Protection de l'Atmosphère. Available at: http://www.airparif.asso.fr/_pdf/publications/Rppa.pdf (accessed 11.04.14.).

AIRPARIF, 2011. Origine des particules en Île-de-France. Available at: www.airparif.asso.fr/_pdf/publications/rapport-particules-110914.pdf (accessed 11.04.14.).

Allen, L., Lindberg, F., Grimmond, C.S.B., 2011. Global to city scale urban anthropogenic heat flux: model and variability. Int. J. Climatol. 31, 1990–2005.

Amato, F., Pandolfi, M., Escrig, A., Querol, X., Alastuey, A., Pey, J., Perez, N., Hopke, P., 2009. Quantifying road dust resuspension in urban environment by multilinear engine: a comparison with PMF2. Atmos. Environ. 43, 2770–2780.

Appel, K., Roselle, S., Gilliam, R., Pleim, J., 2010. Sensitivity of the Community Multiscale Air Quality (CMAQ) model v4.7 results for the eastern United States to MM5 and WRF meteorological drivers. Geosci. Model Dev. 3, 169–188.

Borge, R., Alexandrov, V., Josedelvas, J., Lumbreras, J., Rodrìguez, E., 2008. A comprehensive sensitivity analysis of the WRF model for air quality applications over the Iberian Peninsula. Atmos. Environ. 42, 8560–8574.

Boylan, J.W., Russell, A.G., 2006. PM and light extinction model performance metrics, goals, and criteria for three-dimensional air quality models. Atmos. Environ. 40, 4946–4959.

Chen, W., Kuze, H., Uchiyama, A., Suzuki, Y., Takeuchi, N., 2001. One-year observation of urban mixed layer characteristics at Tsukuba, Japan using a micro pulse lidar. Atmos. Environ. 35, 4273–4280.

Chou, C.C.K., Lee, C.T., Chen, W.N., Chang, S.Y., Chen, T.K., Lin, C.Y., Chen, J.P., 2007. Lidar observations of the diurnal variations in the depth of urban mixing layer: a case study on the air quality deterioration in Taipei, Taiwan. Sci. Total Environ. 374, 156–166.

Couvidat, F., Debry, É., Sartelet, K., Seigneur, C., 2012. A hydrophilic/hydrophobic organic (H_2O) model: model development, evaluation and sensitivity analysis. J. Geophys. Res. 117, D10304.

Dandou, A., Tombrou, M., Akylas, E., Soulakellis, N., Bossioli, E., 2005. Development and evaluation of an urban parameterization scheme in the Penn State/NCAR Mesoscale Model (MM5). J. Geophys. Res. 110, D10102.

De Meij, A., Gzella, A., Cuvelier, C., Thunis, P., Bessagnet, B., Vinuesa, J., Menut, L., Kelder, H., 2009. The impact of MM5 and WRF meteorology over complex terrain on CHIMERE model calculations. Atmos. Chem. Phys. 9, 6611–6632.

Debry, É., Fahey, K., Sartelet, K., Sportisse, B., Tombette, M., 2007. Technical note: a new SIze REsolved Aerosol Model (SIREAM). Atmos. Chem. Phys. 7, 1537–1547.

Dudhia, J., 1993. A nonhydrostatic version of the Penn State NCAR Mesoscale Model: validation tests and simulation of an Atlantic cyclone and cold front. Mon. Weather Rev. 121, 1493–1513.

Dupont, E., Menut, L., Carissimo, B., Pelon, J., Flamant, P., 1999. Comparison between the atmospheric boundary layer in Paris and its rural suburbs during the ECLAP experiment. Atmos. Environ. 33, 979–994.

EEA, 2006. EMEP/CORINAIR Emission Inventory Guidebook, 2006 Technical report No 11/2006 Available at: http://www.eea.europa.eu/publications/EMEPCORINAIR4 (accessed 11.04.14.).

Flamant, C., Pelon, J., Flamant, P.H., Durand, P., 1997. Lidar determination of the entrainment zone thickness at the top of the unstable marine atmospheric boundary layer. Bound.-Layer Meteorol. 83, 247–284.

Guibert, S., Matthias, V., Schulz, M., Bösenberg, J., Eixmann, R., Mattis, I., Pappalardo, G., Perrone, M.R., Spinelli, N., Vaughan, G., 2005. The vertical distribution of aerosol over Europe–synthesis of one year of EARLINET aerosol

lidar measurements and aerosol transport modeling with LMDzT-INCA. Atmos. Environ. 39, 2933–2943.
Hanna, S.R., Paine, R.J., 1989. Hybrid plume dispersion model (HPDM) development and evaluation. J. Appl. Meteorol. 28, 206–224.
Hong, S.Y., Noh, Y., Dudhia, J., 2006. A new vertical diffusion package with an explicit treatment of entrainment processes. Mon. Weather Rev. 134, 2318–2341.
Hong, S.Y., Pan, H.L., 1996. Nonlocal boundary layer vertical diffusion in a medium-range forecast model. Mon. Weather Rev. 124, 2322–2339.
Kaufman, Y., Tanré, D., Léon, J.F., Pelon, J., 2003. Retrievals of profiles of fine and coarse aerosols using lidar and radiometric space measurements. IEEE Trans. Geosci. Remote Sens. 41, 1743–1754.
Kim, Y., Couvidat, F., Sartelet, K., Seigneur, C., 2011. Comparison of different gas-phase mechanisms and aerosol modules for simulating particulate matter formation. J. Air Waste Manage. Assoc. 61, 1–9.
Kim, Y., Fu, J.S., Miller, T.L., 2010. Improving ozone modeling in complex terrain at a fine grid resolution – Part II: influence of schemes in MM5 on daily maximum 8-h ozone concentrations and RRFs (Relative Reduction Factors) for SIPs in the non-attainment areas. Atmos. Environ. 44, 2116–2124.
Kim, Y., Sartelet, K., Raut, J.C., Chazette, P., 2013. Evaluation of the weather research and forecast/urban model over Greater Paris. Bound.-Layer Meteorol. 149, 105–132.
Kim, Y., Sartelet, K., Seigneur, C., 2009. Comparison of two gas-phase chemical kinetic mechanisms of ozone formation over Europe. J. Atmos. Chem. 62, 89–119.
Kusaka, H., Kondo, H., Kikegawa, Y., Kimura, F., 2001. A simple single-layer urban canopy model for atmospheric models: comparison with multi-layer and slab models. Bound.-Layer Meteorol. 101, 329–358.
Louis, J.F., 1979. A parametric model of vertical eddy fluxes in the atmosphere. Bound.-Layer Meteorol. 17, 187–202.
Mallet, V., Quélo, D., Sportisse, B., Ahmed de Biasi, M., Debry, É., Korsakissok, I., Wu, L., Roustan, Y., Sartelet, K., Tombette, M., Foudhil, H., 2007. Technical note: the air quality modeling system Polyphemus. Atmos. Chem. Phys. 7, 5479–5487.
Mallet, V., Sportisse, B., 2006. Uncertainty in a chemistry-transport model due to physical parameterizations and numerical approximations: an ensemble approach applied to ozone modeling. J. Geophys. Res. 111, D01302.
Martilli, A., Clappier, A., Rotach, M.W., 2002. An urban surface exchange parameterisation for mesoscale models. Bound.-Layer Meteorol. 104, 261–304.
Menut, L., Flamant, C., Pelon, J., Flamant, P.H., 1999. Urban boundary-layer height determination from lidar measurements over the Paris area. Appl. Opt. 38, 945–954.
Monahan, E.C., Spiel, D.E., Davidson, K.L., 1986. A model of marine aerosol generation via whitecaps and wave disruption. In: Oceanic Whitecaps and Their Role in Air-sea Exchange Processes. D. Reidel, Netherlands, pp. 167–174.
Nakanishi, M., Niino, H., 2004. An improved Mellor Yamada Level-3 model with condensation physics: its design and verification. Bound.-Layer Meteorol. 112, 1–31.
Pleim, J.E., 2011. Comment on "Simulation of surface ozone pollution in the Central Gulf Coast region using WRF/Chem model: sensitivity to PBL and land surface physics". Adv. Meteorol. 2011 article ID 464753, 3 pages.
Raut, J.C., Chazette, P., 2009. Assessment of vertically-resolved PM_{10} from mobile lidar observations. Atmos. Chem. Phys. 9, 8617–8638.
Real, E., Sartelet, K., 2011. Modeling of photolysis rates over Europe: impact on chemical gaseous species and aerosols. Atmos. Chem. Phys. 11, 1711–1727.
Roustan, Y., Sartelet, K., Tombette, M., Debry, É., Sportisse, B., 2010. Simulation of aerosols and gas-phase species over Europe with the Polyphemus system. Part II: model sensitivity analysis for 2001. Atmos. Environ. 44, 4219–4229.
Royer, P., Chazette, P., Sartelet, K., Zhang, Q.J., Beekmann, M., Raut, J.C., 2011. Comparison of lidar-derived PM_{10} with regional modeling and ground-based observations in the frame of MEGAPOLI experiment. Atmos. Chem. Phys. 11, 10705–10726.
Russell, A., Dennis, R., 2000. NARSTO critical review of photochemical models and modeling. Atmos. Environ. 34, 2283–2324.
Salamanca, F., Krpo, A., Martilli, A., Clappier, A., 2010. A new building energy model coupled with an urban canopy parameterization for urban climate simulations - Part I. formulation, verification, and sensitivity analysis of the model. Theor. Appl. Climatol. 99, 331–344.
Sartelet, K.N., Debry, É., Fahey, K., Roustan, Y., Tombette, M., Sportisse, B., 2007. Simulation of aerosols and gas-phase species over Europe with the Polyphemus system: Part I–Model-to-data comparison for 2001. Atmos. Environ. 41, 6116–6131.
Seinfeld, J., Pandis, S., 1998. Atmospheric Chemistry and Physics: from Air Pollution to Climate Change. Wiley-Interscience, New York.
Shin, H., Hong, S.Y., 2011. Intercomparison of planetary boundary-layer parametrizations in the WRF model for a single day from CASES-99. Bound.-Layer Meteorol. 139, 261–281.
Simpson, D., Fagerli, H., Jonson, J., Tsyro, S., Wind, P., Tuovinen, J.P., 2003. Transboundary Acidification Eutrophication and Ground Level Ozone in Europe. Part I. Unified EMEP model description EMEP status report 1/03 Part I Available at: http://emep.int/publ/reports/2003/emep_report_1_part1_2003.pdf (accessed 11.04.14.).
Simpson, D., Winiwarter, W., Börjesson, G., Cinderby, S., Ferreiro, A., Guenther, A., Hewitt, C.N., Janson, R., Aslam, M., Khalil, K., Owen, S., Pierce, T.E., Puxbaum, H., Shearer, M., Skiba, U., Steinbrecher, R., Tarrasón, L., Öquist, M.G., 1999. Inventorying emissions from nature in Europe. J. Geophys. Res. 104, 8113–8152.
Tang, W., Cohan, D.S., Morris, G.A., Byun, D.W., Luke, W.T., 2011. Influence of vertical mixing uncertainties on ozone simulation in CMAQ. Atmos. Environ. 45, 2898–2909.
Troen, I.B., Mahrt, L., 1986. A simple model of the atmospheric boundary layer; sensitivity to surface evaporation. Bound.-Layer Meteorol. 37, 129–148.
Uno, I., Ueda, H., Wakamatsu, S., 1989. Numerical modeling of the nocturnal urban boundary layer. Bound.-Layer Meteorol. 49, 77–98.
Yarwood, G., Rao, S., Yocke, M., Whitten, G., 2005. Updates to the Carbon Bond Chemical Mechanism: CB05 Final Report to the US EPA. RT-0400675 Available at: http://www.camx.com/publ/pdfs/CB05_Final_Report_120805.pdf (accessed 11.04.14.).